

Potential of a neutral impurity in a large ^4He cluster

KEVIN K. LEHMANN†

JILA, University of Colorado and National Institute of Standards and Technology,
Boulder, CO 80309–0440, USA

(Received 16 June 1998; revised version accepted 28 April 1999)

This paper presents an analysis of the motion of a neutral impurity species in a nanometre scale ^4He cluster, extending a previous study of the dynamics of an ionic impurity. It is shown that for realistic neutral impurity–He potentials, such as those of SF_6 and OCS , the impurity is kept well away from the surface of the cluster by long range induction and dispersion interactions with He, but that a large number of ‘particle in a box’ centre-of-mass states are thermally populated. It is explicitly demonstrated how to calculate the spectrum that arises from the coupling of the impurity rotation and the centre-of-mass motion, and it is found that this is a potentially significant source of inhomogeneous broadening in vibration–rotation spectra of anisotropic impurities. Another source of inhomogeneous broadening is the hydrodynamic coupling of the rotation of the impurity with the centre-of-mass velocity. A quantum hamiltonian to describe this effect is derived from the classical hydrodynamic kinetic energy of an ellipsoid. Simple analytic expressions are derived for the resulting spectral line shape for an impurity in bulk He, and the relevant matrix elements derived to allow fully quantum calculations of the coupling of the centre-of-mass motion and rotation for an impurity confined in a spherical He cluster. Lastly, the hydrodynamic contribution to the impurity effective moment of inertia is evaluated and found to produce only a minor fractional increase.

1. Introduction

The last few years have seen dramatic advances in the spectroscopy of atoms and molecules attached to large He clusters [1]. These clusters provide an unique environment for a spectroscopy which combines many of the attractive features of both high resolution gas phase spectroscopy and traditional matrix spectroscopy [2]. These include the ability to obtain rotationally resolved spectra of even very large molecules such as SF_6 [3] and $(\text{CH}_3)_3\text{SiCCH}$ [4] (though with effective rotational constants only $\frac{1}{3}$ – $\frac{1}{5}$ as large as those of the gas phase molecule), and the ability to form and stabilize extremely fragile species [5], including high spin states of molecules. Particularly interesting is the recent demonstration by Grebenev *et al.* [6] that the free rotation is a direct consequence of the boson character of ^4He , and can be viewed as a microscopic version of the famous Andronikashvili experiment [7] that was used to measure the superfluid fraction in bulk liquid He.

Despite rapid progress, many fundamental questions remain about spectroscopy in this environment. One such important question is the origin of the linewidth observed in ro-vibrational spectra. These linewidths vary with species, from 150 MHz reported for the R(0)

line of the OCS ν_3 fundamental band [8], to 1.5cm^{-1} reported for H_2O [9]. Very recently, pure microwave spectra have been observed for impurity molecules (CH_3CN and HCCCN) which have linewidths on the order of 1 GHz [10]. Since this is comparable to linewidths observed in ro-vibrational transitions, it is unlikely that vibrational dephasing, which is the dominant line broadening mechanism in the spectra of impurities in classical liquids, also plays a dominant role in He cluster spectroscopy. Likewise, vibrational population relaxation, which has been invoked as the source of line broadening, obviously cannot contribute to the broadening in the case of microwave excitation.

Given the fact that the He clusters are uniquely fluid, even down to zero temperature, it is natural to suppose that the impurity spectra will not display inhomogeneous effects. Variations in local binding sites tend to dominate the linewidth of spectra in low temperature crystal or glass hosts. In a liquid environment, local changes in solvation lead to dynamic fluctuations in the spectral intervals, and thus can lead to dephasing but not static inhomogeneous effects. Since the time scale for solvation fluctuations, due to the large zero point kinetic energy of He atoms in the bulk, is expected to be much faster than the dephasing times observed in most ro-vibrational spectra, one can expect the effects of the fluctuating solvation to be strongly motionally averaged. More fundamentally, it is far from clear that we

† 1998 Visiting Fellow. Permanent address: Department of Chemistry, Princeton University, Princeton NJ 08544, USA.

expect pure vibrational dephasing at all given the low temperature of He clusters. Taking the model of a crystalline solid, one expects dephasing to arise from interactions with thermal excitations. Since, as will be discussed below, the only excitations thermally excited are surface waves, and these are expected to interact extremely weakly with impurities, it is difficult to see how dephasing can be important.

The fact that the existing experiments produce a broad distribution of cluster sizes suggests an inhomogeneous contribution to the line broadening from a size dependent shift in the absorption. However, it is likely that this effect is also not dominant in most spectra. First, the overall shift of the ro-vibrational line from the gas phase to He clusters is fairly small, typically at most a few cm^{-1} [1], so the spread in shifts as one approaches the bulk limit is expected to be small. Below, an estimate of the expected shift of the SF_6 ν_3 vibrational transition due to the finite size of the He cluster will be given. Further, the experimentalist has some control over the mean of the cluster size distribution. In previous work on SF_6 , it was found that the spectral shift and temperature was essentially constant for He clusters of $> 10^3$ He atoms [8].

An additional source of inhomogeneous environment needs to be considered, the distribution of the position and orientation of the impurity relative to the surface of the cluster. That this could be relevant is suggested by the following simple calculation. Consider an impurity with an effective mass (including hydrodynamic contributions) of 50 atomic mass units (u) in equilibrium with a He cluster, which is known to be at 0.38 K [3]. This molecule will have a root mean squared (RMS) velocity of 14 m s^{-1} . In a cluster of diameter 10 nm, which corresponds to $\approx 11\,000$ He atoms, it will take $\approx 0.7 \text{ ns}$ for the impurity to cross the cluster. If the scattering of the impurity from the surface of the cluster leads to re-orientational dephasing, the resulting line broadening will be $\approx 500 \text{ MHz}$, comparable to what has been observed in ro-vibrational transitions [1]. An additional source of dephasing is the hydrodynamic coupling of the molecular orientation to the molecular velocity, which will be described in more detail below.

The simplest treatment for the motion of the impurity molecule is as a ‘particle in a box’. This was considered in an earlier paper by Toennies and Vilesov [11]. Their treatment was unsatisfactory on several grounds however. First, as we will demonstrate below, the true potential is not really ‘flat’ inside the box relative to the low value of the thermal energy. Second perhaps more importantly, they did not attempt to calculate the intensity of transitions in this model. Since the effective potential is almost the same in the upper and lower vibrational states, there are small Frank–Condon factors for transi-

tions that change the centre-of-mass quantum numbers of the impurity, and as such, changes in energy of the particle-in-a-box levels are not directly observable in the spectrum of a neutral impurity.

This paper will present a model that allows calculation of the effective potential for the motion of an impurity that is free to move about in a spherical liquid He droplet of radius R . A thorough analysis of the liquid drop model for pure He clusters was provided by Brink and Stringari [12]. The present calculation will be based upon long range interactions and treat the He as a continuum incompressible liquid of constant number density, ρ , which we will take as the known value of bulk liquid He. While such a model cannot be expected to correctly describe the interaction of the impurity with the first few solvation shells, this solvation structure is expected to be effectively constant as long as the impurity does not too closely approach the surface of the cluster. For realistic values of the impurity–He long range interaction, the energetics are effective at keeping the impurity from this difficult region. Further, since the impurity is kept away from the edge of the cluster, the fact that the He cluster has a diffuse ($\approx 7 \text{ \AA}$) interface with vacuum [13] will not be expected to significantly affect the impurity potential. Further, we can, with good approximation, keep only the lowest order terms in the expansion of the long range He–impurity interaction in inverse powers of distance.

The paper is organized as follows. Section 2 will consider a neutral, isotropic impurity, with SF_6 used as an example. Sections 3 and 4 will consider the case of a symmetric top or linear molecule impurity, with HCN used as an example. Section 3 will derive the effective potential and apply a classical model for calculation of the resulting spectra. Section 4 will derive the matrix elements needed for a fully quantum treatment of the interaction of the centre-of-mass motion and the rotations of the impurity for a linear molecule, leading to a calculation of the expected spectral structure for the case of the HCN R(0) rotational line. Section 5 will consider the effect of the interaction of an impurity with the internal modes of the cluster, deriving the expected shifts produced by the interaction with the riplons, which are quantized surface capillary waves. These interactions are found to be completely negligible contributions to the linewidth of transitions. Section 6 will consider hydrodynamic effects and derive the effective hamiltonian and matrix elements for the hydrodynamic coupling of the rotation and centre-of-mass momentum of the impurity. When this model is applied to the HCN R(0) line, poor agreement is found with experiment. However, it will be shown in section 7 that the combination of the anisotropic potential terms and hydrodynamic coupling leads to a prediction for the lineshape

of the R(0) line in the OCS ro-vibrational spectrum that is in excellent agreement with that observed in helium clusters and reported by Toennies' group [14]. Section 8 will examine the hydrodynamic contribution to the reduction in rotational constant for an impurity, treated as an ellipsoid. It is found that the hydrodynamic kinetic energy only makes a minor contribution to the observed increase in moment of inertia of impurity molecules. Lastly, section 9 will provide an overview and summary of this work.

2. Isotropic neutral impurity, such as SF₆, in a helium cluster

In a previous paper [15], the potential of an ionic impurity in a helium cluster was derived from the ion-induced dipole interaction of the impurity in helium. The present paper will consider the case of a neutral impurity. As will be shown, this potential is dominated by the leading power in the long range interaction between the impurity and atomic helium. In the present section, the case of an impurity that has an isotropic long range interaction with He will be considered. This will be the case for impurity molecules of tetrahedral or octahedral symmetry as well as for atomic impurities. In the next section, the case of an anisotropic long range interaction, as expected for a linear molecule impurity, will be treated.

As in our previous paper, we will take as a reference of energy not an isolated impurity atom or molecule, but the impurity in bulk He with constant He number density, ρ . In this way, the difference between an impurity inside the cluster and our reference state is the absence in the later case of He outside the cluster. We will also implicitly assume that the impurity is far enough away from the surface of the He cluster that we treat the interaction of the impurity with this 'missing' He as pairwise additive and we can use only the long range terms of the potential.

Let the interaction energy of the impurity with the He be a van der Waals attraction at long range, with a long range form of:

$$V(r) = -\frac{C_6}{r^6} - \frac{C_8}{r^8} \dots, \quad (1)$$

where C_6 and C_8 are the long range dispersion interaction constants and r is the distance from the centre of mass of the impurity to the He atom. For SF₆, the lowest order anisotropic term appears at the r^{-10} level.

Consider the impurity to be displaced from the centre of a He cluster of radius R by a distance a . The z axis is defined as parallel to the displacement vector of the impurity from the centre of the cluster, which provides the origin for the coordinate system. Let $r(\theta)$ be the distance from the impurity to the droplet surface at a

polar angle θ measured from the impurity. Basic trigonometry gives:

$$R^2 = (a + r \cos(\theta))^2 + r^2 \sin^2(\theta) = a^2 + r^2 + 2ar \cos(\theta) \quad (2)$$

from which we can derive:

$$r(\theta) = [R^2 - a^2 \sin^2(\theta)]^{1/2} - a \cos(\theta). \quad (3)$$

We can 'sum' up the missing interaction for all the He atoms absent (compared to the bulk phase) due to the finite extent of the cluster, using the interaction potential given above in equation (1):

$$\begin{aligned} \Delta E(a, R) &= \int_0^\pi \int_{r(\theta)}^\infty \left[\frac{\rho C_6}{r'^6} + \frac{\rho C_8}{r'^8} \right] 2\pi r'^2 \sin(\theta) dr' d\theta \\ &= V_2^0 F_2(a/R) + V_3^0 F_3(a/R), \end{aligned} \quad (4)$$

$$V_2^0 = \left(\frac{4\pi\rho C_6}{3R^3} \right), \quad (5)$$

$$F_2(y) = [1 - y^2]^{-3} \approx 1 + 3y^2 + 6y^4 + 10y^6 + \dots, \quad (6)$$

$$V_3^0 = \left(\frac{4\pi\rho C_8}{5R^5} \right), \quad (7)$$

$$F_3(y) = \frac{1 + \frac{5}{3}y^2}{(1 - y^2)^5} \approx 1 + \frac{20}{3}y^2 + \frac{70}{3}y^4 + 60y^6, \dots \quad (8)$$

We will consistently use $y = a/R$ in this paper and refer to y as the normalized displacement of the impurity. We start with label F_2 to avoid confusion with the function F_1 defined in the paper on ionic impurities [15].

In atomic units, the C_6 and C_8 coefficients are typically of the same magnitude [16], and thus we expect V_3^0 to be smaller than V_2^0 by a factor on the order of $a_0^2/R^2 \approx 10^{-4}$ (a_0 is the Bohr radius), and thus we will neglect it. Using the C_6 coefficient for SF₆-He equal to $35 E_h a_0^6 = 3.35 \times 10^{-78} \text{ J m}^6$ [17] (E_h is the Hartree, the atomic unit of energy), $\rho = 0.022 \text{ atoms } \text{\AA}^{-3}$ (the density of liquid He at low pressure and temperature), and $R = 3 \text{ nm}$ (which corresponds to the size of a cluster containing ≈ 2500 He atoms), we calculate $V_2^0 = 0.572 \text{ cm}^{-1} hc \approx 2k_b T_c$. k_b is Boltzmann's constant and $T_c = 0.38 \text{ K}$ is the temperature of nanometre scale He clusters. If we assume that the effective mass for translational motion of the impurity is $M_{\text{eff}} = 186u$ ($u =$ atomic mass units) (the SF₆ plus 10 He atoms to include hydrodynamic effects and some 'sticking' of solvated He atoms), we get a harmonic frequency for the vibration of the impurity about the centre of the He

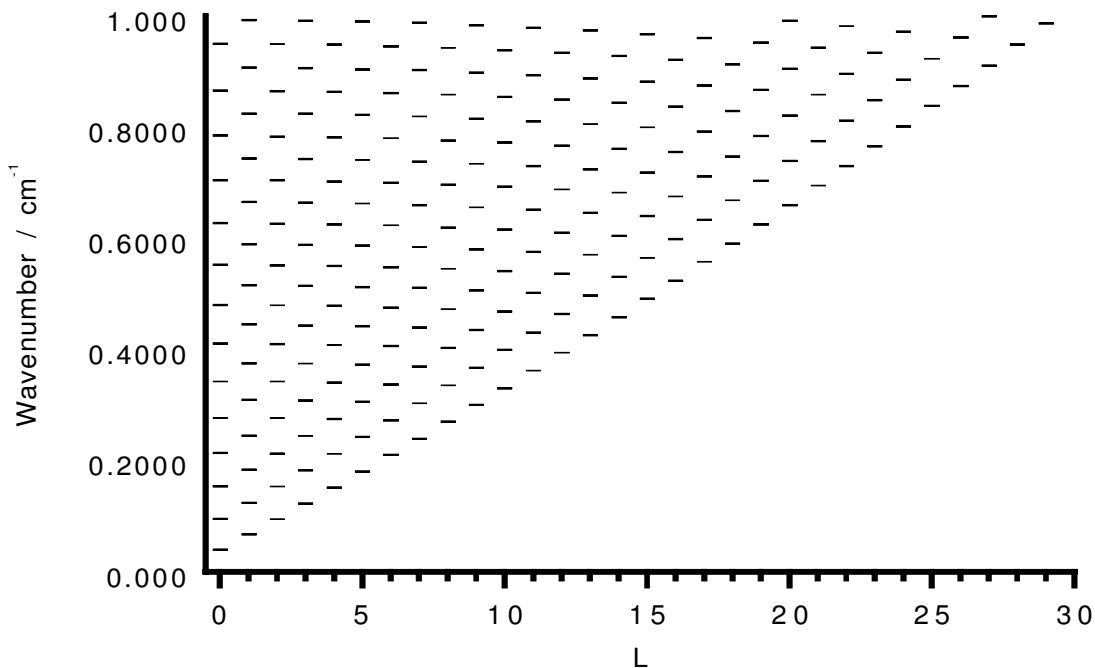


Figure 1. Centre-of-mass motion energy levels for SF₆ in a He cluster of radius 3 nm. All levels below 1 cm⁻¹ are plotted. The ordinate is L , the total orbital angular momentum quantum number with states of increasing n , the number of nodes in the radial direction, increasing vertically in each column.

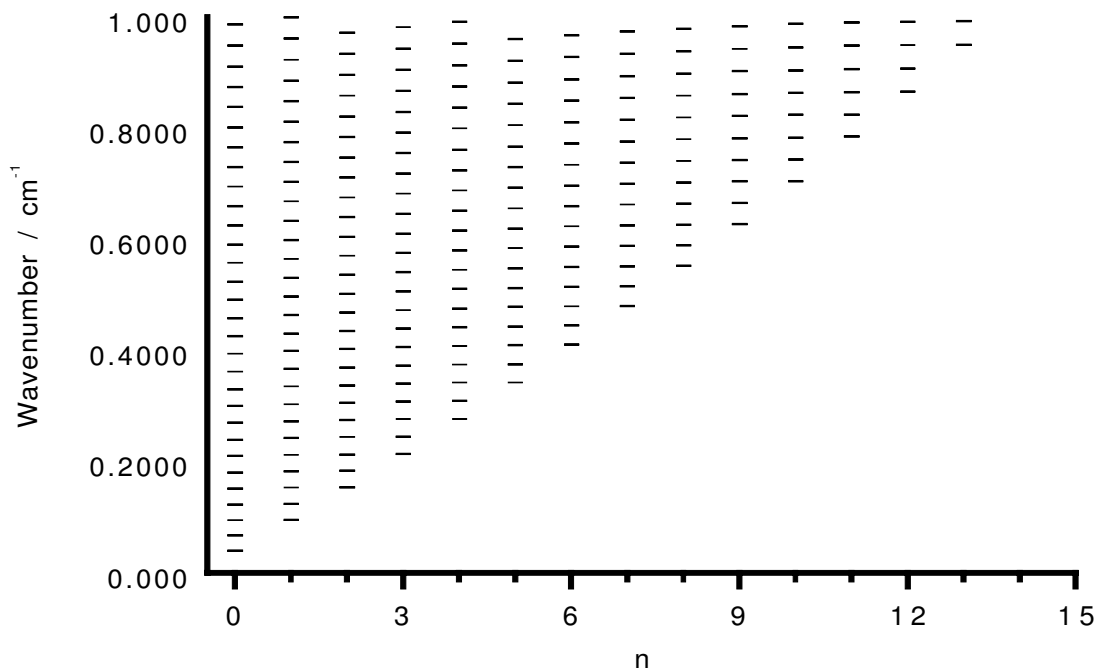


Figure 2. Same as figure 1, but with n as the ordinate and states of increasing L increasing vertically in each column.

cluster of 790 MHz. Figures 1 and 2 show the energy levels of this potential below 1 cm⁻¹ $\approx 4k_b T_c$, calculated using the Numerov–Cooley method [18]. Inspection of the energy as a function of n (radial) and L (angular

momentum) quantum numbers shows that the thermally well populated energy levels have a spectrum much more like that of a particle in a three-dimensional harmonic well than a particle in a spherical ‘box’. Figure 3 con-

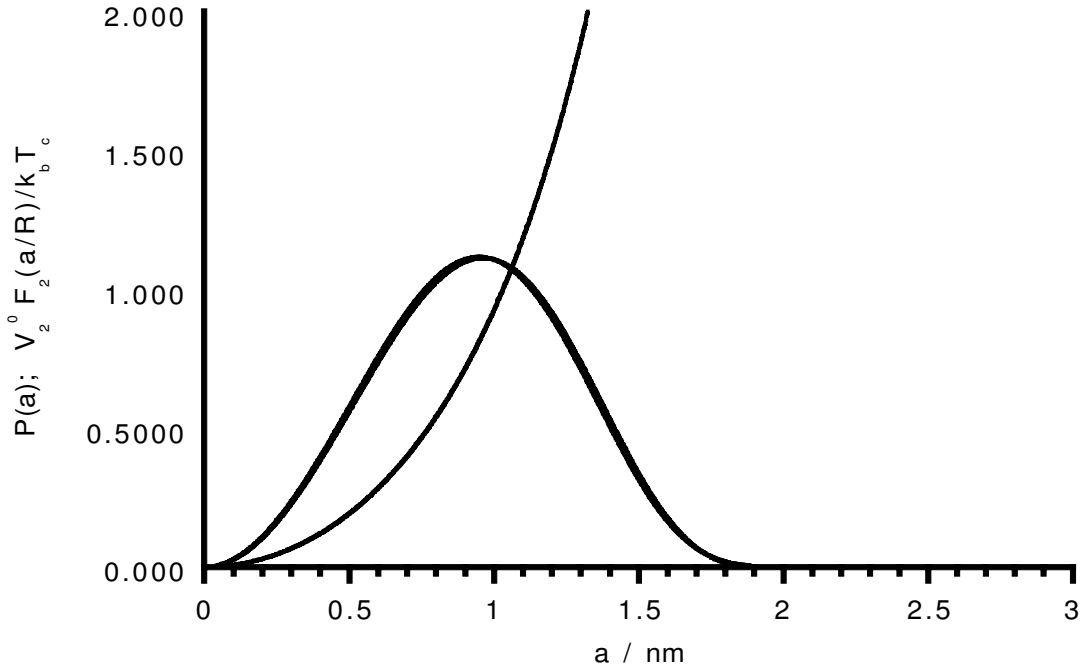


Figure 3. Comparison of the classical and quantum radial distribution functions, $P(a)$, for SF_6 in a 3 nm He cluster. The quantum distributions have been calculated from the set of all eigenstates with a wavenumber less than 2cm^{-1} . Also plotted, is the isotropic potential, $U(a)$, that confines the SF_6 in the cluster.

Table 1. Thermodynamic averages for the motion of SF_6 and riplons in a He cluster at $T_c = 0.38\text{K}$. R is the radius of the cluster, \mathcal{Q} the partition function for the centre-of-mass motion or the riplons, $\langle E \rangle$ is the thermally averaged energy, expressed in units of $k_b T_c$, C_v is the heat capacity in units of k_b , S is the entropy in units of k_b , $\langle L^2 \rangle$ is the mean squared value for the thermal angular momentum, $\langle a^2 \rangle$ is the mean squared value for the displacement of the impurity from the centre of the cluster, and $\langle n \rangle$ is the mean number of quanta of excitation of the riplon modes.

	R/nm	\mathcal{Q}	$\langle E \rangle / (k_b T_c)$	C_v / k_b	S / k_b	$\sqrt{\langle L^2 \rangle}$	$\sqrt{\langle a^2 \rangle} / \text{nm}$	$\langle n \rangle$
SF_6 quantum	3.0	478	2.49	2.01	8.66	16.3		
SF_6 classical	3.0	536	2.44	2.13	8.72	16.4	0.96	
Riplons	3.0	$8.7 \cdot 10^3$	18.6	45.4	30.0	15.2		14.8
SF_6 classical	5.0	$8.2 \cdot 10^4$	2.21	2.06	11.2	39.2	2.9	
Riplons	5.0	$1.1 \cdot 10^{16}$	54.1	127.8	91.1	41.0		54.9

tains a plot of the probability density for finding the impurity a distance a from the from the centre of a $R = 3\text{nm}$ cluster, calculated both from the set of eigenfunctions and from the classical Boltzmann distribution. We see an excellent agreement of the two, confirming the classical character of this motion even at T_c . We see that the probability density is largely localized in the region with a less than about half the cluster radius. The RMS value for the displacement of the impurity from the cluster centre is 0.96nm . The highly classical nature of the thermal motion can also be seen by comparing the thermodynamic functions calculated from the exact quantum energy levels and for classical motion with the same potential. This comparison is shown in table 1. Also included in this table is the mean squared orbital angular momentum (calculated in units of \hbar^2), calcu-

lated as the thermally averaged value of $L(L+1)$, where L is the orbital angular momentum quantum number of the impurity motion around the centre of the cluster, which is compared to the classical thermal mean value of $\langle L^2 \rangle = 2M_{\text{eff}}k_b T_c \langle a^2 \rangle / \hbar^2$. The table also contains the thermodynamic averages for a cluster of $R = 5\text{nm}$ as well as the corresponding properties of the riplons (to be discussed below). It can be seen that the average energy and heat capacity are intermediate between those of a true particle in a box and a particle in a harmonic well. The partition function for translation grows faster than the volume of the cluster, a factor of 15.3 compared to 4.6 when the radius of the cluster is increased from 3 to 5 nm. This reflects the fact that in a larger cluster, the impurity gets to sample thermally a larger fraction of the cluster volume, as

demonstrated by the RMS thermal displacement, $(\langle a^2 \rangle)^{1/2}$.

3. Symmetric top or linear molecule impurity in the helium cluster

We will now assume we have an impurity with an anisotropic interaction with He. If the impurity is in the centre of the cluster, it will experience an isotropic net potential, due to the symmetry of the distribution of He atoms. However, as the impurity moves away from the centre, it will experience an anisotropic potential. This anisotropy will cause a coupling between the centre-of-mass motion of the impurity and its rotational motion, and can be expected to result in orientational dephasing. It is of interest to point out that the thermal mean value of the orbital angular momentum (L) of the impurity in the cluster $\approx 20\hbar$ is much greater than the thermally populated value of rotational angular momentum of the impurity, j , and as a consequence the procession of j about the total angular momentum J would be expected to completely dephase the average dipole moment, and lead to line broadening.

The long range interaction of a neutral, symmetric top impurity with He can be written as the sum of two parts, one due to induction and the other dispersion. The former is dominated by the dipole-induced dipole interaction for an impurity with a permanent dipole moment. We can write the potential in the following form [19]:

$$V(r, \phi) = -\frac{C_{60}}{r^6} - \frac{C_{62}}{r^6} P_2(\cos(\phi)) - \frac{C_{71}}{r^7} P_1(\cos(\phi)) - \frac{C_{73}}{r^7} P_3(\cos(\phi)), \quad (9)$$

where P_n are the Legendre polynomials, and ϕ is the angle between the vector from the centre of mass of the impurity to the He, and the symmetry axis of the impurity. The induction contributions to these coefficients can be calculated [19] from the dipole moment, μ , and quadrupole moment, Θ , of the impurity and the polarizability, α , of He:

$$C_{60}^{\text{ind}} = C_{62}^{\text{ind}} = \frac{\alpha\mu^2}{(4\pi\epsilon_0)^2}, \quad (10)$$

$$C_{73}^{\text{ind}} = \frac{2}{3} C_{71}^{\text{ind}} = \frac{12\alpha\mu\Theta}{5(4\pi\epsilon_0)^2}. \quad (12)$$

The dispersion contributions to the long range interactions can be written as integrals over the imaginary frequency dependent polarizability of He and the polarizability and dipole-quadrupole polarizabilities of the impurity [20]. The polarizability is higher parallel than perpendicular to the bonds. As a result, for linear molecules and most prolate symmetric tops, $C_{62} > 0$, which

means that for such impurities, the interaction is lower in energy when the He-impurity displacement is parallel rather than perpendicular to the impurity symmetry axis.

As an example, we will consider the case of HCN as the impurity. Using the parameters $\alpha(\text{He}) = (4\pi\epsilon_0) 1.383 a_0^3$, $\mu(\text{HCN}) = 1.174 ea_0 = 2.98$ Debye, and $\Theta(\text{HCN}) = 1.777 ea_0^2$ [19], we get that the induction contribution to the long range coefficients are: $C_{60}^{\text{ind}} = C_{62}^{\text{ind}} = 1.14 \text{ eV } \text{\AA}^6$ and $C_{73}^{\text{ind}} = \frac{2}{3} C_{71}^{\text{ind}} = 2.19 \text{ eV } \text{\AA}^7$. The dispersion contributions to the coefficients have been calculated by Atkins and Hutson [19] to be $C_{60}^{\text{disp}} = 7.81 \text{ eV } \text{\AA}^6$, $C_{62}^{\text{disp}} = 1.11 \text{ eV } \text{\AA}^6$, $C_{71}^{\text{disp}} = 4.93 \text{ eV } \text{\AA}^7$, and $C_{73}^{\text{disp}} = 1.19 \text{ eV } \text{\AA}^7$.

To find the effective potential of the impurity in the cluster, we will once again integrate the above effective long range interaction (equation (9)) over the He atoms ‘missing’ from the cluster. As before, we define the z axis as along the displacement of the molecule from the centre of the cluster. We also define χ as the angle between the symmetry axis of the impurity and this z axis. In terms of these coordinates, we have the angle, ϕ , between this impurity symmetry axis and the vector from the impurity to a point in space as:

$$\cos(\phi(\mathbf{r}')) = \sin(\theta) \cos(\varphi) \sin(\chi) + \cos(\theta) \cos(\chi), \quad (12)$$

where θ and φ are the spherical coordinates of the point \mathbf{r}' defined relative to the position of the impurity. The results of the integration give the following results for the effective potential for the impurity:

$$\begin{aligned} \Delta E(a, R, \chi) = & V_2^0 F_2(a/R) + V_4^0 F_4(a/R) P_2(\cos(\chi)) \\ & + V_5^0 F_5(a/R) \cos(\chi) \\ & + V_6^0 F_6(a/R) P_3(\cos(\chi)), \end{aligned} \quad (13)$$

$$V_4^0 = \frac{4\pi\varphi C_{62}}{3R^3}, \quad (14)$$

$$\begin{aligned} F_4(y) = & \frac{1}{32} [y(1-y^2)]^{-3} \\ & \times \left[-6y + 16y^3 + 6y^5 + 3(1-y^2)^3 \ln\left(\frac{1+y}{1-y}\right) \right], \end{aligned} \quad (15)$$

$$V_5^0 = \frac{4\pi\varphi C_{71}}{3R^4}, \quad (16)$$

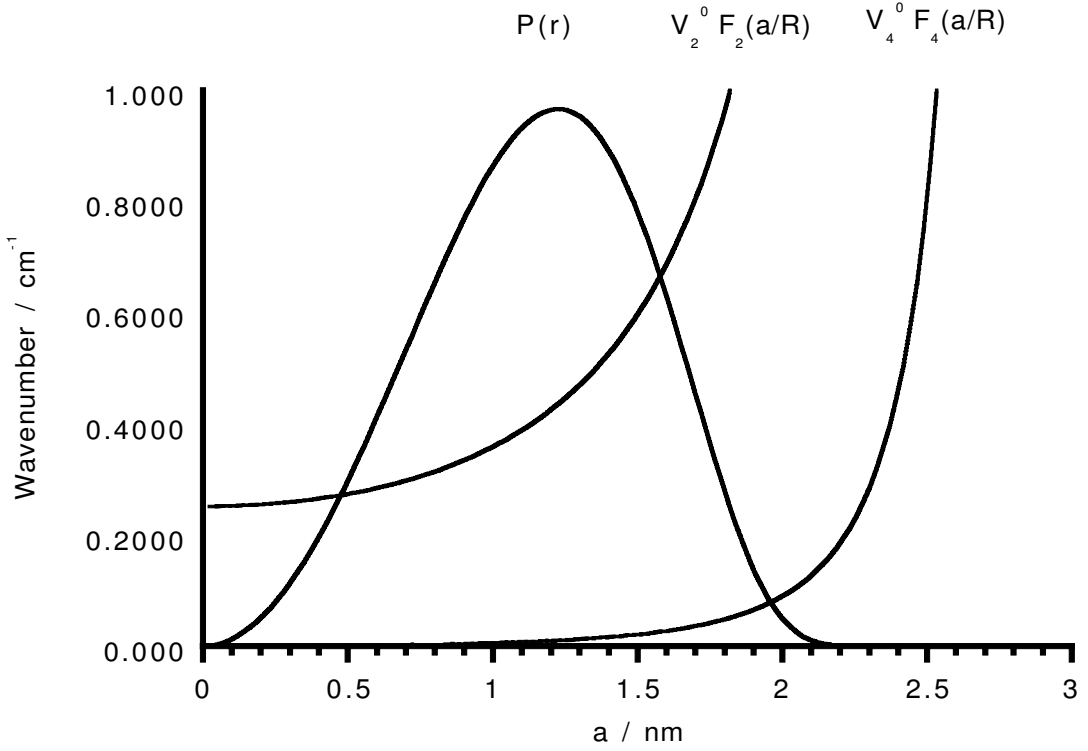


Figure 4. Comparison of isotropic (P_0) and anisotropic (P_2) potentials for an HCN impurity in a helium cluster of 3 nm radius.

$$F_5(y) = \frac{y}{(1-y^2)^4}, \quad (17)$$

$$V_6^0 = \frac{4\pi\rho C_{73}}{3R^4}, \quad (18)$$

$$F_6(y) = \frac{15}{256} [y(1-y^2)]^{-4} \times \left[2y^7 + \frac{146}{15}y^5 - \frac{22}{3}y^3 + 2y - \ln\left(\frac{1+y}{1-y}\right)(y^8 - 4y^6 + 6y^4 - 4y^2 + 1) \right]. \quad (19)$$

$F_2(y)$ and V_2^0 are unchanged from the previous definitions. Despite the rather singular appearance of $F_4(y)$ and $F_6(y)$ near $y \approx 0$, they are regular:

$$F_4(y) \approx \frac{3}{5}y^2 + \frac{12}{7}y^4 + \frac{10}{3}y^6 \dots, \quad (20)$$

$$F_5(y) \approx y + 4y^3 + 10y^5 \dots, \quad (21)$$

$$F_6(y) \approx \frac{15}{35}y^3 + \frac{15}{9}y^5 \dots \quad (22)$$

If we consider the case of HCN in a He cluster of $R = 3$ nm, and use the parameters given above, we get for the effective potential:

$$\Delta E(a, R, \chi) \frac{1}{hc} = (0.2519F_2(y) + 0.0045F_5(y) \cos(\chi)) + 0.0619F_4(y)P_2(\cos(\chi)) + 0.0031F_6(y)P_3(\cos(\chi)) \text{ cm}^{-1}. \quad (23)$$

We see that the two C_7 terms ($F_5(y)$ and $F_6(y)$) can be neglected in first approximation compared to the isotropic and leading anisotropic term ($F_2(y)$ and $F_4(y)$) that derive from the C_6 terms. These coefficients are comparable to the line widths observed in ro-vibrational spectra of molecules inside He clusters. The V_2^0 isotropic term will confine the impurity near the centre of the cluster. As discussed above, this term determines the effective potential for the translational motion of the impurity, while the weaker anisotropic term will couple the translational motion to the rotation of the impurity molecule. Figure 4 shows a plot of these two terms as a function of a for the case considered here, along with a plot of the thermal probability density distribution as calculated from the isotropic potential, $V_2^0 F_2(y)$. It can be seen that the anisotropic term, $V_4^0 F_4(y)$, is much smaller than the isotropic term over the full range of displacements that are thermally well populated.

Since $C_{60} > 0$, it is lower in energy for the HCN axis to be perpendicular to the displacement from the centre

of the cluster ($\phi = \pi/2$). This is easily rationalized if one considers the case of HCN below a flat He surface. When $\phi = \pi/2$, the nearest ‘missing helium’ is perpendicular to the HCN molecular axis, and this costs less energy than when $\phi = 0$. If the interaction energy is much weaker than the separation of rotational levels of the impurity, which will be the case for HCN for all the thermally well populated configurations, to first order we can consider the effective potential for translational motion to be the average of the effective potential over the rotational function of the impurity. For a linear molecule, the odd Legendre terms average to zero, while the P_2 term will split the m_j degeneracy of each j level, such that the centre of gravity is conserved. If we consider the impurity centre-of-mass displacement as static, then the natural axis of quantization of the angular momentum is parallel to this displacement, with an energy of a j, m_j rotational state equal to:

$$\Delta E(a, J, M) = V_2^0 F_2(a/R) + V_4^0 F_4(a/R) \left(\frac{j(j+1) - 3m_j^2}{(2j-1)(2j+3)} \right), \quad (24)$$

which implies that $m_j = 0$ states have the highest energy and $m_j = j$ the lowest of each manifold of fixed j states.

A proper quantum mechanical treatment of the coupling of the rotation and translational motion of an anisotropic impurity will be given in the next section. This section will close by demonstrating a simple ‘classical’ application of the above results to estimate a line broadening mechanism in the case of SF₆. The ground state of SF₆ has octahedral symmetry, and thus has only an isotropic long range interaction, as discussed above. However, the infrared (IR) allowed vibrational excitations are triply degenerate levels. The ν_3 mode observed in the IR spectrum of SF₆ in He clusters has a particularly large vibrational transition dipole moment of $\mu_3 = 0.388$ Debye for the $\nu_3 = 0 \rightarrow 1$ transition. As the SF₆ is displaced in the ν_3 mode, it will have a dipole moment proportional to normal coordinate Q_3 . This dipole result in a dipole-induced dipole interaction with the He, which modifies the force constant for this normal mode [21]. The modification of the ν_3 wavenumber (relative once again to SF₆ in bulk liquid He), as a function of the position of the SF₆ in the cluster and the orientation of the triply degenerate ν_3 mode are given by equations (10) and (13), with the derivative of the dipole with respect to the dimensionless normal coordinate (which is just $2^{1/2}$ larger than the fundamental transition dipole moment) replacing the permanent dipole moment. If we treat these coordinates classically, we can calculate the spectrum of the ν_3 mode of SF₆ in the cluster, relative to SF₆ in bulk

liquid He from the effective potential. Thus, we can write $\nu_3(a, \chi)$ as

$$\nu_3(a, R, \chi) = \nu_3(\infty) + \nu^0 [F_2(a/R) + F_4(a/R) P_2(\cos(\chi))], \quad (25)$$

$$\nu^0 = \frac{(\epsilon_r - 1) 2\mu_3^2}{12\pi\epsilon_r^2\epsilon_0 R^3}. \quad (26)$$

$\nu_3(\infty)$ is the frequency of ν_3 in the bulk He limit and χ is the angle between the displacement of the SF₆ and the direction of polarization of the ν_3 mode. Note that this expression would be exact if a did not change in time, i.e. we have a static inhomogeneous distribution of impurity positions, as in a matrix without diffusion. Dynamic motion of a and χ will tend to motionally average the instantaneous frequency $\nu_3(a(t), \chi(t))$ and lead to a narrower spectrum than predicted by this approximation, which is sometimes known as the ‘statistical method’ [22] and was first introduced by Kuhn and London [23] to model pressure broadening.

For the case of the ν_3 mode of SF₆ in an $R = 3$ nm He cluster, $\nu^0 = 16$ MHz. Since the isotropic term, $F_2(y)$ dominates over the anisotropic term, $F_4(y)$, over the range of impurity displacements that are thermally populated, we will keep only the isotropic term. We can write the spectral density, $S(\nu)$ as

$$S(\nu_3) = \left(\frac{d\nu_3}{da} \right)^{-1} Z_c^{-1} 4\pi\omega^2 \exp(-V_2^0 F_2(y)/k_b T_c) \quad (27)$$

$$= \frac{24\pi R}{Z_c} [1 - \lambda^{-1}]^{3/2} \lambda^4 \exp \left[-\frac{V_2^0}{k_b T_c} \lambda^9 \right], \quad (28)$$

$$\lambda(\nu_3) = \left(\frac{\nu_3 - \nu(\infty)}{\nu^0} \right)^{1/3}, \quad (29)$$

where $Z_c = \int_0^R 4\pi\omega^2 \exp(-V_2^0 F_2(a/R)/k_b T_c) da$. Figure 5 shows the calculated spectral lineshape for ν_3 of SF₆ in this model. It can be observed that the residual shift of the mode (compared to the limit of SF₆ in bulk He) and the FWHM (full width at half maximum) are both estimated to be about 30 MHz. This can be compared to the linewidth of ≈ 300 MHz FWHM observed by Hartmann *et al.* [3] for the ν_3 mode of SF₆ in ⁴He clusters of mean size 4000 atoms ($R = 3.5$ nm). It is clear that the calculated spectral broadening is more than an order of magnitude below that observed in the laboratory, which argues that this effect contributes at most a minor fraction of the total dephasing rate.

In their earlier paper that considered ‘particle-in-a-box’ states of an impurity in He clusters, Toennies and Vilesov [11] proposed that these levels could be directly

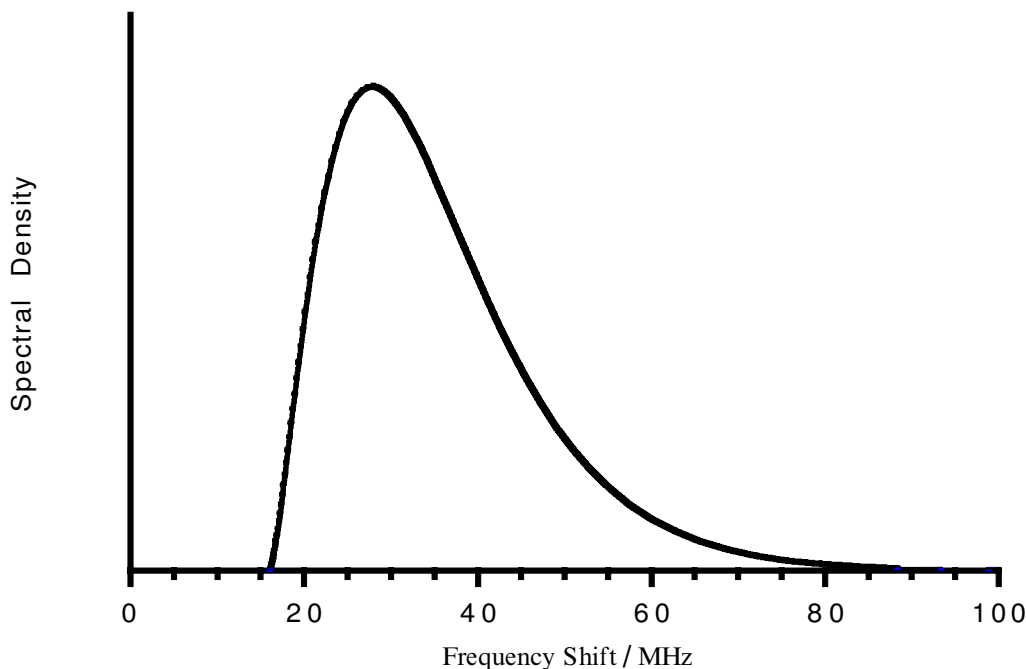


Figure 5. Calculated spectral lineshape for the ν_3 fundamental of SF_6 based upon the dipole-induced dipole spectral shift, which depends upon the position inside the cluster.

observed as satellite lines on a vibrational band of an impurity. They suggested that such particle-in-a-box state changing transitions could gain intensity due to differences in the effective potential in the upper and low vibrational states, but reported no estimate of the expected intensities of such transitions. Using the SF_6 example, the author has calculated Frank–Condon factors for transitions that change the quantum numbers for the centre-of-mass motion along with a vibrational transition. The largest such Frank–Condon factor was below $\sim 10^{-4}$. This is not unexpected since the excited state has an effective potential that is stronger by only $\approx 0.1\%$. Based upon this analysis, it appears unlikely that such centre-of-mass motion changing transitions will be directly observed unless the change in potential with vibrational coordinate is much larger. It is worth pointing out that the spectral structure that Toennies and Vilesov suggested may be due to such transitions was later assigned by them to the rotational structure of the vibrational transition inside the He cluster [3].

4. Interaction of impurity translational and rotational motions

Because the interaction between the impurity and the He cluster depends upon both the position of the impurity in the cluster and the orientational angles of the impurity, there is a coupling that can lead to relaxation of the orientational order, and thus line broadening in the impurity spectra. The purpose of

this section is to elaborate how this can be calculated. While the physical origin of the effect is quite different, this problem has some mathematical similarity to the coupling of rotation and translation that has been used to model the IR spectra of light rotors in solid noble-gas matrices [24–27]

We will assume our impurity is free to move in the cluster with an effective mass M_{eff} . We will further assume it to be a linear molecule with an effective rotational constant B_{eff} in helium. We will model the system with the hamiltonian:

$$H = -\frac{\hbar^2}{2M_{\text{eff}}}\nabla^2 + B_{\text{eff}}\mathbf{j}^2 + V_2^0 F_2(y) + V_4^0 F_4(y) P_2(\cos(\theta_{12})). \quad (30)$$

In this equation, ∇^2 operates on the centre-of-mass coordinates of the impurity, \mathbf{j} is the angular momentum operator for rotation of the impurity and θ_{12} is the angle between the displacement of the impurity from the centre of the cluster and the direction of the linear axis of the impurity. The results are easily extended to include other Legendre terms, such as those that arise from the r^{-7} terms in the long range potential of an isolated impurity and He atom.

If we keep all but the last term in our zero order hamiltonian, then rotational and translational motion are separable and we can write wavefunctions as:

$$|n, j, m_j, L, M_L\rangle = \frac{\chi_{n,L}(a)}{a} Y_{j,m_j}(\Omega_1) Y_{L,M_L}(\Omega_2), \quad (31)$$

where $\chi_{n,L}(a)$ are the numerical solutions to the radial potential, $V_2^0 F_2(y)$, with orbital angular momentum quantum number, L . $\Omega_1 = \theta_1, \phi_1$ are the orientational angles of the rotor, and $\Omega_2 = \theta_2, \phi_2$ the angles of the centre of mass of the impurity, but referenced to some arbitrary laboratory fixed axis system. Introduction of the $V_4^0 F_4(y) P_2$ term will couple j and L , to form a total angular momentum J . We can write the basis function of the coupled representation as:

$$|n, j, L, J, M\rangle = (-1)^{j-L} (2J+1)^{1/2} \sum_{m_1, m_2} \begin{pmatrix} j & L & J \\ m_1 & m_2 & -M \end{pmatrix} \times |n, j, m_1, L, m_2\rangle. \quad (32)$$

The matrix elements of the zero order hamiltonian are diagonal in this representation as well, and given by:

$$E_{n,j,L}^0 = E_{n,L}^0 + B_{\text{eff}} j(j+1). \quad (33)$$

The $E_{n,L}^0$ and $\chi_{n,L}(a)$ can be determined by numerical solution (using the Numerov-Cooley method) of the radial Schrödinger equation.

The coupling matrix elements can be calculated using standard methods of angular momentum theory [28, 29], including the Spherical Harmonic Addition Theorem to write $P_2(\cos(\theta_{ij}))$ in terms of products of spherical harmonics of coordinates Ω_1 and Ω_2 :

$$\begin{aligned} \langle n, j, L, J, M | H' | n', j', L', J, M \rangle \\ = V_4^0 \langle n, L | F_4(r) | n', L' \rangle (-1)^{J+j+L'} \\ \times [(2j+1)(2j'+1)(2L+1)(2L'+1)]^{1/2} \\ \times \begin{pmatrix} j & j' & 2 \\ 0 & 0 & 0 \end{pmatrix} \begin{pmatrix} L & L' & 2 \\ 0 & 0 & 0 \end{pmatrix} \left\{ \begin{matrix} J & j & L \\ 2 & L' & j' \end{matrix} \right\}. \quad (34) \end{aligned}$$

The two $3J$ symbols in this expression lead to the selection rules for coupling that $j' = j, j \pm 2$ and $L' = L, L \pm 2$. Explicit expressions for all the required $3J$ and $6J$ symbols can be found in the tables given by Edmonds [28]. Since for the cases considered at present, the coupling matrix elements are comparable to the separation of the centre-of-mass motion states, but are much less than the separations of the rotational energy levels of the impurity, the matrix elements that are off diagonal in j are neglected in numerical calculations presented below.

The only change needed for other Legendre terms is to replace the '2' in the above equations by the order of the Legendre term, and the radial integral will be over

the appropriate function, $F_n(y)$. These terms will loosen the selection rule on Δj and ΔL for states that can be coupled. Parity, which is determined by $(-1)^{j+L}$, will remain a good quantum number.

In order to calculate the dipole transition moments, we will treat the electric field as along the laboratory Z axis. This gives:

$$\begin{aligned} \langle Y_{j,m_1} | \cos(\theta) | Y_{j',m_1} \rangle = [(2j+1)(2j'+1)]^{1/2} (-1)^{m_1} \\ \times \begin{pmatrix} j & j' & 1 \\ 0 & 0 & 0 \end{pmatrix} \begin{pmatrix} j & j' & 1 \\ -m_1 & m_1 & 0 \end{pmatrix}, \quad (35) \end{aligned}$$

where θ is the angle between the Z axis and the symmetry axis of the impurity molecule. Going to the coupled representation we have:

$$\begin{aligned} \langle n, j, L, J, M | \cos(\theta) | n', j', L', J', M' \rangle \\ = (-1)^{j+j'+L+M+1} \delta_{n,n'} \delta_{L,L'} \delta_{M,M'} \\ \times [(2j+1)(2j'+1)(2J+1)(2J'+1)]^{1/2} \\ \times \begin{pmatrix} j & j' & 1 \\ 0 & 0 & 0 \end{pmatrix} \begin{pmatrix} J & J' & 1 \\ -M & M & 0 \end{pmatrix} \left\{ \begin{matrix} L & j' & J' \\ 1 & J & j \end{matrix} \right\}. \quad (36) \end{aligned}$$

We can expand the eigenfunctions in terms of the functions of the coupled representation as:

$$|k, J, M\rangle = \sum_{n,j,L} |n, j, L, J, M\rangle \langle n, j, L, J | k, J \rangle \quad (37)$$

(k is a label to distinguish eigenstates with the same total angular momentum quantum numbers). We do not put the M label on the amplitudes since these are independent of M due to rotational invariance. We can define a line strength factor for the intensity of a transition between two levels k, J and k', J' as follows:

$$S(k, J; k', J') = 3 \sum_{M, M'} |\langle k, J, M | \cos(\theta) | k', J', M' \rangle|^2 \quad (38)$$

by exploiting the normalization of $3J$ symbols, we can reduce this to:

$$\begin{aligned} S(k, J; k', J') = (2J+1)(2J'+1) \\ \times \left[\sum_{n,j,j',L} \langle k, J | n, j, L, J \rangle \langle n, j', L, J' | k', J' \rangle \right. \\ \times [(2j+1)(2j'+1)]^{1/2} \\ \left. \times (-1)^{j+j'+L} \begin{pmatrix} j & j' & 1 \\ 0 & 0 & 0 \end{pmatrix} \begin{pmatrix} L & j' & J' \\ 1 & J & j \end{pmatrix} \right]^2. \quad (39) \end{aligned}$$

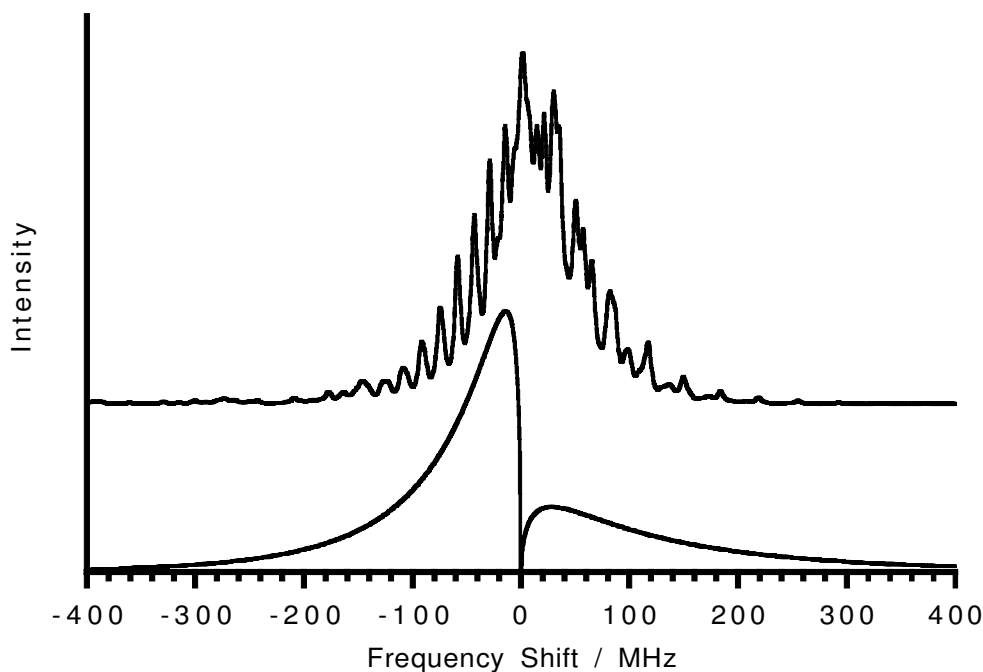


Figure 6. Simulation of the HCN R(0) transition in a 3 nm radius helium cluster, using the anisotropic potential discussed in the text, including coupling between the HCN rotation and its centre-of-mass motion relative to the centre of the He cluster.

Figure 6 shows a simulation of the $j = 0 \rightarrow 1$ rotational transition of HCN in a $R = 3$ nm He cluster. The calculated ‘stick’ spectrum has been convoluted with a Lorentzian lineshape with FWHM of 3 MHz. A spectral broadening of the transition of ≈ 150 MHz can be seen in the figure. The residual ‘fine’ structure would be washed out when one does an average over the experimental cluster size distribution in a simulation of a real experiment, but the overall FWHM of the transition is not a strong function of cluster size. Also shown in the figure is the lineshape calculated from the semi-classical ‘statistical’ spectral model, where the spectrum is calculated as a Boltzman average over different ‘static’ centre-of-mass positions for the HCN. The two ‘bumps’ correspond to $J, M = 0, 0 \rightarrow 1, \pm 1$ (more intense low frequency side) and $\rightarrow 1, 0$ (broader and less intense high frequency bump). These individual transitions are ‘washed out’ in the full quantum spectrum because the motion of the impurity causes the natural quantization axis (the direction of the displacement from the centre of the cluster) to average over all directions. The linewidth observed for the R(0) line in the first C–H overtone band of HCN is ≈ 1.0 GHz, an order of magnitude larger. This suggests that another mechanism dominates the dephasing rate in the experiment.

Recently, Nauta and Miller [30] have observed the R(0) transition in the C–H fundamental band of HCN. They find that the lineshape consists of two features, with a width and separation in qualitative agree-

ment with the above ‘statistical’ model, i.e. as predicted without motional averaging. Furthermore, they have studied the spectrum as a function of external electric field, and have found that the two features correlate with the two high field $m = \pm 1$ and $m = 0$ peaks expected for the R(0) transition of a polar linear molecule.

5. Interaction of impurity with He cluster excitations

Up to now, we have considered the effect of the cluster potential on the rotational and translational degrees of freedom of an impurity. We will now consider the interaction of the impurity with the internal vibrational excitations of the He cluster. These can be separated into two types. The first are bulk excitations that consist of density fluctuations or phonons. The second are surface excitations that consist of capillary waves and are known as riplons.

As discussed by Brink and Stringari [12], for a cluster of N atoms, the lowest phonon excitation, the symmetric breathing mode, has a frequency of $540N^{-1/3}$ GHz. Even for a cluster of $N = 10^4$ He atoms, this corresponds to 25 GHz which is much larger than $k_b T_c / h = 8.0$ GHz. Thus, only a few percent of such clusters have any quanta of excitation in the phonon modes. This implies that such modes cannot produce a significant level of inhomogeneous broadening in impurity spectra. It is possible to observe excitations of the phonon modes in an impurity absorption spectrum, but such excitations should appear as a well sepa-

rated ‘phonon side band’ which peaks several cm^{-1} to the blue of the ‘zero phonon line’ which does not involve phonon excitations. Such phonon wings are commonly seen in the electronic spectra of impurities in He [31, 32], but have not yet been observed in impurity vibration–rotation spectra. This is presumably due to a small change in effective He solvation around impurities following vibrational excitation. As a result, almost all the transition intensity is concentrated in the zero phonon line.

In contrast, the lowest frequency surface waves have much lower wavenumbers, and excitations are thermally excited even at the low temperature of He clusters. These excitations involve no change in He density and the only restoring force is due to the increase in surface area caused by the change in the surface shape. The theory of such surface waves is presented in the classic text *Hydrodynamics* by Lamb [33], and discussed, in the context of He clusters, by Brink and Stringari [12], who calculated the spectra and thermodynamic functions of these excitations as a function of cluster size.

Due to excitation of ripples, the surface of the He cluster develops oscillations. If we consider a point of the surface of the cluster at polar angles θ_s, ϕ_s (again, relative to some arbitrary laboratory fixed coordinate system), we can write the displacement of the surface as:

$$r(\theta_s, \phi_s) = R + \sum_{L_s, M_s} S(L_s, M_s) Y_{L_s, M_s}(\theta_s, \phi_s). \quad (40)$$

In the above equation, $S(L_s, M_s)$ is the normal coordinate of the surface wave with angular momentum quantum numbers L_s, M_s . The theory assumes that $S(L_s, M_s) \ll R$. The sum is for $L_s \geq 2$. The functions for $L_s = 0$ correspond to the breathing mode, and $L_s = 1$ corresponds to a translation of the entire cluster, not distortions of the cluster shape. If we assume that the surface tension of He is $\sigma = 380 \mu\text{J m}^{-2}$ [12], the frequency of the L_s, M_s surface mode is independent of M_s and is given by:

$$\begin{aligned} \nu(L_s) &= \frac{\omega(L_s)}{2\pi} = \frac{1}{2\pi} \left[L_s(L_s - 1)(L_s + 2) \frac{\sigma}{M_{\text{He}} \rho R^3} \right]^{1/2} \\ &= \left[L_s(L_s - 1)(L_s + 2) \frac{\sigma}{3\pi M_{\text{He}}} \right]^{1/2} N^{-1/2} \\ &= 78 \text{ GHz} [L_s(L_s - 1)(L_s + 2)]^{1/2} N^{-1/2}. \end{aligned} \quad (41)$$

For a cluster of size $N = 10^4$, $\nu(L_s = 2) = 2.2 \text{ GHz}$. The clusters will have a maximum value of $(L_s)_{\text{max}} \approx (\pi/2) N^{1/3}$ which is estimated by assuming that the smallest wavelength is approximately twice the mean interparticle distance. For a cluster of $R = 3 \text{ nm}$,

this corresponds to $(L_s)_{\text{max}} = 26$. Table 1 presents thermal average quantities for the ripples in clusters of sizes $R = 3$ and 5 nm , which can be compared with the thermal averages of the impurity centre-of-mass motion presented. Note that the average energy and entropy in the ripples greatly exceeds that of the impurity and forms the dominant ‘heat bath’ of the cluster. However, the average thermal angular momentum in the impurity centre-of-mass motion approximately equals the total in the ripples. We can thus anticipate that in coming to equilibrium, the angular momentum constraints may play an important role. It is also worth noting that for a cluster of size $R = 3 \text{ nm}$, the total canonical internal energy at T_c is about equal to the energy required to evaporate a single He atom, $\approx 18.8 k_b T_c$ [12]. Thus, one can anticipate that smaller clusters will be slightly warmer than larger clusters, due to their low heat capacity. This is in contrast to the fact that we expect a slight decrease in He binding energy for smaller clusters, and thus higher vapour pressure, which would argue that smaller clusters should be colder. The decrease in binding energy, due to change in surface free energy, can be estimated as $2\sigma/(\rho R) = 1.73 \text{ cm}^{-1} \text{ nm}/R$, and is considerably larger than the increase in binding energy caused by attraction to a neutral impurity, which is $\approx 0.17 \text{ cm}^{-1} \text{ nm}^6/R^6$ for the case of SF₆.

We can model the interaction between an impurity and a ripplon by considering the change in the sum of impurity–He interactions caused by the modulation in the surface of the cluster. Let $\delta r(\theta_s, \phi_s)$ be the modulation in the cluster radius in the direction (θ_s, ϕ_s) measured from the centre of the cluster. (Note: this is a change from our previous treatments where we used polar angles defined from the impurity.) As above, let y equal the normalized distance of the impurity from the centre of the cluster. To first order in δr , we can write the change in He–impurity interactions as:

$$\begin{aligned} U(y) &= \frac{C_{60}\rho}{R^4} \int \frac{\delta r(\Omega_s) d\Omega_s}{[1 + y^2 - 2y \cos(\theta_{\text{is}})]^3} \\ &\quad + \frac{C_{62}\rho}{R^4} \int \frac{\delta r(\Omega_s) P_2(\cos(\theta_{\text{isr}}) d\Omega_s}{[1 + y^2 - 2y \cos(\theta_{\text{is}})]^3}, \end{aligned} \quad (42)$$

where C_{60} and C_{62} are the isotropic and anisotropic contributions of the C_6 coefficients, Ω_s is the surface solid angle, θ_{is} is the angle between the vector from the centre of the cluster to the impurity and the vector from the centre of the cluster to the surface, and θ_{isr} is the angle between the vector from the impurity to the point on the surface in the direction θ_s, ϕ_s from the centre of the cluster and the vector along the symmetry axis of the impurity. It is also useful to introduce the

additional quantities as follows: r_{is} , the distance from the impurity to the surface; θ_{ir} , the angle between the vector from the centre to the impurity and the vector along the axis of the impurity; and θ_{sr} , the angle between the vector from the centre to the surface and the vector along the axis of the impurity. We can write these angles in terms of the three sets of polar angles for the impurity centre of mass (θ_i, φ_i), the surface (θ_s, φ_s), and the rotor (θ_r, φ_r) as follows:

$$\cos(\theta_{\text{is}}) = \cos(\theta_i) \cos(\theta_s) + \sin(\theta_i) \sin(\theta_s) \cos(\varphi_i - \varphi_s), \quad (43)$$

$$\cos(\theta_{\text{ir}}) = \cos(\theta_i) \cos(\theta_r) + \sin(\theta_i) \sin(\theta_r) \cos(\varphi_i - \varphi_r), \quad (44)$$

$$r_{\text{is}} = a[1 + y^2 - 2y \cos(\theta_{\text{is}})]^{1/2}, \quad (45)$$

$$\cos(\theta_{\text{isr}}) = \frac{a}{r_{\text{is}}} [\cos(\theta_{\text{sr}}) - y \cos(\theta_{\text{ir}})]. \quad (46)$$

An exact treatment of this model would consider the simultaneous interaction of the surface waves, the centre-of-mass motion of the impurity, and the rotation of the impurity, each of which has its own angular momenta that must be coupled. We will consider here instead a model for the interaction of the ripples and impurity rotation alone. As such, we will treat the impurity as fixed at some normalized distance, y , from the centre of the cluster in a direction we will select for the z axis. In the end, we will predict the spectrum by averaging over the possible positions y , using a Boltzmann weighting. In this approximation we have $\cos(\theta_{\text{is}}) = \cos(\theta_s)$ and $\cos(\theta_{\text{ir}}) = \cos(\theta_r)$. In order to predict the $j=0 \rightarrow 1$ rotational transition of the impurity, we will need to average the interaction over the lowest rotational functions of the rotor. This gives:

$$\langle Y_{00}(\Omega_r) | P_2(\cos(\theta_{\text{isr}})) | Y_{00}(\Omega_r) \rangle = 0, \quad (47)$$

$$\begin{aligned} & \langle Y_{10}(\Omega_r) | P_2(\cos(\theta_{\text{isr}})) | Y_{10}(\Omega_r) \rangle \\ &= \frac{1}{5} \left[\frac{3 \cos^2(\theta_s) - 4y \cos(\theta_s) + 2y^2 - 1}{1 + y^2 - 2y \cos(\theta_s)} \right], \quad (48) \end{aligned}$$

$$\begin{aligned} & \langle Y_{1\pm 1}(\Omega_r) | P_2(\cos(\theta_{\text{isr}})) | Y_{1\pm 1}(\Omega_r) \rangle \\ &= -\frac{1}{2} \langle Y_{10}(\Omega_r) | P_2(\cos(\theta_{\text{isr}})) | Y_{10}(\Omega_r) \rangle. \quad (49) \end{aligned}$$

We thus find that the $j=0$ rotor state does not couple to the ripples, while the $j=1$ state does.

In order to calculate matrix elements of the interaction, we need to determine the dimensionless amplitude for the ripplon vibrations. Using the methods

presented in Lamb's text [33], we can determine the effective mass, $\mu(L_s)$, for each ripplon:

$$\mu(L_s) = \frac{M_{\text{He}} \rho R^3}{L_s}. \quad (50)$$

Note that the effective mass is proportional to the total mass of the cluster, not the mass of atoms near the surface. This is due to the fact that the surface waves have a velocity field that goes into the bulk of the cluster, with the velocity proportional to y^{L_s-1} . Surface waves of higher L_s values are increasingly confined to motion of atoms closer to the surface, and thus have a reduced effective mass. Using this relationship, we can write the surface displacement in terms of raising and lowering operators for the ripples ($a^\dagger(L_s, M_s)$ and $a(L_s, M_s)$) as follows:

$$\delta r(\theta_s, \varphi_s) = \sum_{L_s, M_s} S(L_s, M_s) Y_{L_s, M_s}(\theta_s, \varphi_s), \quad (51)$$

$$S(L_s, M_s) = d_s(L_s) \left(a^\dagger(L_s, M_s) + a(L_s, M_s) \right), \quad (52)$$

$$\begin{aligned} d_s(L_s) &= \left[\frac{\hbar}{2\mu(L_s)\omega(L_s)} \right]^{1/2} \\ &= \left[\frac{L_s \hbar^2}{2(L_s - 1)(L_s + 2)\sigma M_{\text{He}} \rho R^3} \right]^{1/4}. \quad (53) \end{aligned}$$

For $R = 3$ nm, $d_s(2) = 0.37$ Å. Summing the thermally averaged displacement of all ripples up to $(L_s)_{\text{max}}$ gives a RMS thermal motion of the surface of $1.34(1.50)$ Å for clusters of $R = 3(5)$ nm radii.

We can thus write the interaction of ripples with the rotation of the impurity molecule as follows:

$$\begin{aligned} \mathcal{H}_{\text{ripple, rotation}} &= U_0 \sum_{L_s, M_s} \left(a^\dagger(L_s, M_s) + a(L_s, M_s) \right) \\ &\quad \times \left(\frac{L_s}{(L_s - 1)(L_s + 2)} \right)^{1/4} \\ &\quad \times \int \frac{Y_{L_s, M_s}(\Omega_s) P_2(\cos(\theta_{\text{isr}})) d\Omega_s}{[1 + y^2 - 2y \cos(\theta_{\text{is}})]^3}, \quad (54) \end{aligned}$$

$$U_0 = \left(\frac{C_{60} \rho}{R^4} \right) \left[\frac{\hbar^2}{2\sigma M_{\text{He}} \rho R^3} \right]^{1/4}. \quad (55)$$

For a HCN impurity in a 5 nm He cluster, $U_0 = 1.3$ MHz h .

Despite the fact that the integral diverges as $y \rightarrow 1$, the coupling matrix elements diagonal in rotational quantum numbers are much less than the spacing between ripplon states for the range of y that includes most of the probability density of the impurity. Since the

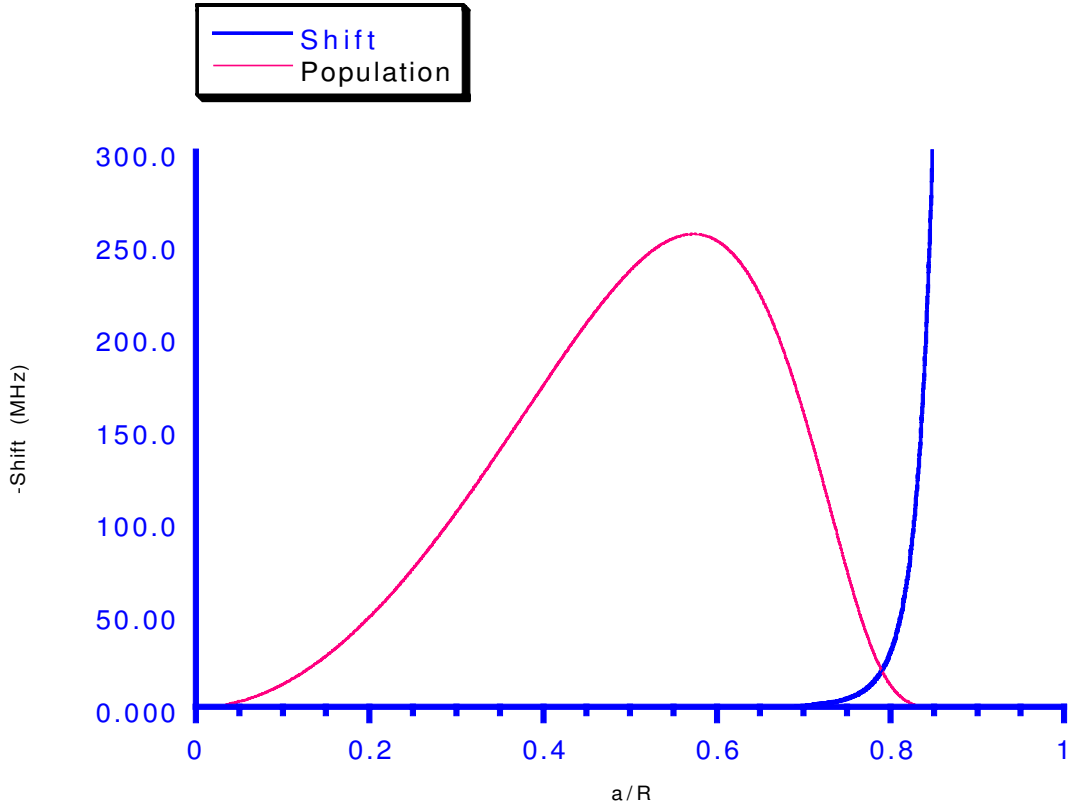


Figure 7. Calculated shift in HCN $j = 1$, $m_j = 0$ level as a result of the interaction with the surface riplons, as a function of impurity displacement from the centre of the cluster. Also plotted is the radial distribution function in arbitrary units to show the region of thermal population.

coupling is linear in the ripplon coordinates (which are harmonic oscillators), $\mathcal{H}_{\text{riplon,rotation}}$ has no first order contribution to the energy. This suggests that we can treat this coupling by second order perturbation theory to account for the virtual creation and annihilation of riplons as an impurity rotates. A consequence of the linear ripplon coupling is that this second order correction is independent of the occupation of the ripplon modes! Such coupling shifts the equilibrium position of the riplons from zero displacement but does not change their force constant. We find a shift in energy equal to:

$$\begin{aligned} \Delta E(y, j, m_j) &= \sum_{L_s, M_s} -\frac{U_0^2}{h\nu(L_s)} \left(\frac{L_s}{(L_s - 1)(L_s + 2)} \right)^{1/2} \\ &\times \left[\int \frac{Y_{L_s, M_s}(\Omega_s) \langle Y_{j, m_j}(\Omega_r) | P_2(\cos(\theta_{\text{isr}})) | Y_{j, m_j}(\Omega_r) \rangle d\Omega_s}{[1 + y^2 - 2y \cos(\theta_{\text{is}})]^3} \right]^2. \end{aligned} \quad (56)$$

If we select the z axis as along the vector from the centre of the cluster to the impurity centre of mass, then only the $M_s = 0$ terms contribute to the sum.

The above expression was used to calculate the shift in the energy of the $j = 1$, $m_j = 0$ level as a function of y . The integrals over θ_s were performed numerically using Gauss–Legendre integration. The shift for the two $j = 1$, $m_j = \pm 1$ levels will be just one quarter as large. Figure 7 shows the calculated shift divided by Planck's constant as a function of a , along with a plot of the radial distribution function for the impurity. This was calculated from the isotropic, C_{60} , interaction energy, as described above. It can be seen that the ripplon induced shift is completely negligible except for the extreme tail of the Boltzmann distribution. We can conclude that the potential interaction of the impurity rotation with the riplons can be neglected compared to the position dependent anisotropic dispersion interaction.

6. Hydrodynamic coupling of impurity motions

While the motions of the impurity in the superfluid He are expected to be without friction, the medium does exert an influence by hydrodynamic effects. The reason

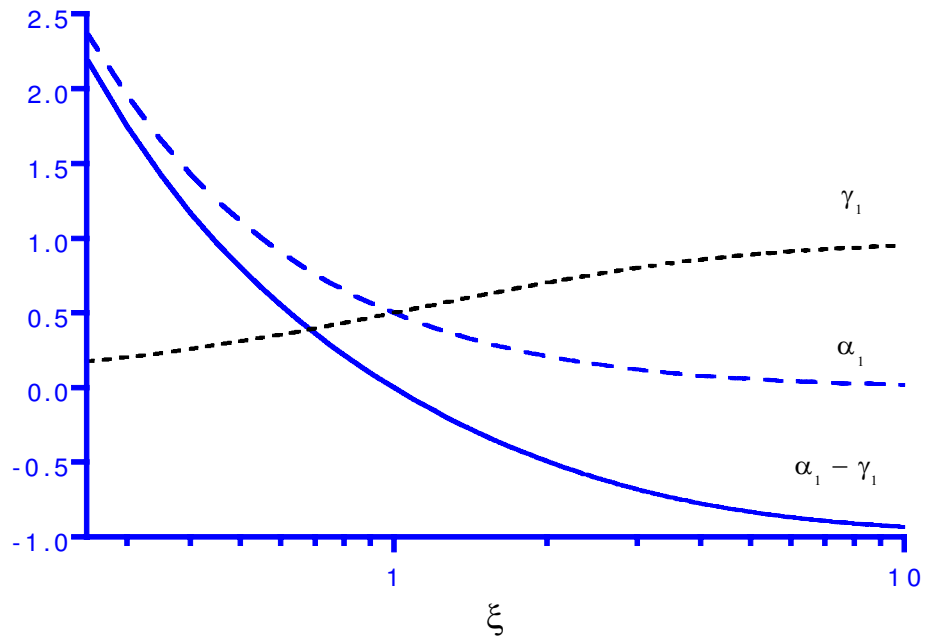


Figure 8. The hydrodynamic constants α_1 and γ_1 and their difference as a function of ξ , which is the ratio of the size of the ellipsoid along the symmetry axis divided by the size perpendicular to this.

is that as the impurity rotates or translates, He atoms must move out of the way to avoid the short range repulsion. For a spherical impurity, the effect of the He kinetic energy produced by the impurity translational motion can be modelled by an effective mass for the impurity that is increased by 0.5 times the mass of He displaced by the impurity. For an anisotropic impurity, there is in addition both a hydrodynamic contribution to the effective moment of inertia for rotation, and a coupling between rotation and centre-of-mass motion. In this section a detailed calculation of these effects will be presented. This type of coupling was previously discussed (though developed in much less detail) in a paper by Elser and Platzman, who proposed an anisotropic solvation structure around positive ions in bulk liquid He to explain an observed temperature dependence to the effective mass of ions [34].

The hydrodynamic coupling of translation and rotation does not occur for an impurity with tetrahedral or octahedral symmetry [33]. Let us model the impurity molecule as a rigid, symmetric ellipsoid of principal axes $a = b = 3.2 \text{ \AA}$ and $c = \xi a = 3.7 \text{ \AA}$. These parameters are based upon the position of the inner wall in the He–HCN potential of Atkins and Hutson [19]. Since the dominant hydrodynamic effect is for parts of the fluid close to the moving body, the use of a continuum, incompressible fluid model is a questionable approximation. However, because of its simplicity, it is worth working out in detail the predictions of this model. Further, it may be the case that the form of

the resulting hamiltonian may be more generally applicable than the simple hydrodynamic model used to derive it.

The motion of an ellipsoid in an incompressible fluid without viscosity is worked out in the text by Milne-Thomson [35]. The hydrodynamic kinetic energy is given for an ellipsoid moving in any direction relative to its principal axes. \mathbf{v} denotes the velocity of the ellipsoid relative to the fluid at large distance from the ellipsoid; $\boldsymbol{\lambda}$ denotes a unit vector in the direction of the unique principal axis; $M' = M_{\text{He}} \rho \frac{4}{3} \pi a^3 \xi$ is the mass of He displaced by the ellipsoid (34.6 u for the HCN–He parameters given above), and M the mass of the ellipsoid. The classical kinetic energy of translational motion of the ellipsoid is:

$$T = \frac{1}{2}(M + \frac{1}{3}M'(2\gamma_1 + \alpha_1))\mathbf{v} \cdot \mathbf{v} + \frac{1}{2}M'(\alpha_1 - \gamma_1) \times [(\boldsymbol{\lambda} \cdot \mathbf{v})^2 - \frac{1}{3}\mathbf{v} \cdot \mathbf{v}], \quad (57)$$

where

$$\alpha_1 = \frac{\alpha_0}{2 - \alpha_0}, \quad \gamma_1 = \frac{\gamma_0}{2 - \gamma_0}, \quad (58)$$

$$\alpha_0 = \int_0^\infty \frac{\xi dx}{(1+x)(\xi^2+x)^{3/2}},$$

$$\gamma_0 = \int_0^\infty \frac{\xi dx}{(1+x)^2(\xi^2+x)^{1/2}}. \quad (59)$$

Figure 8 shows α_1 , γ_1 , and their difference as a function of ξ . We can see that the coupling between translational motion and rotation is zero in the case of a sphere

($\xi = 1$), saturates for a very prolate ellipsoid ($\xi \gg 1$), and diverges for an extremely oblate ellipsoid ($\xi \rightarrow 0$), i.e. for a flat disc. For our model of HCN in He, $\xi = 1.16$, and we have $\alpha_1 = 0.419$ and $\gamma_1 = 0.544$. The coupling of λ and \mathbf{v} reflects the fact that it takes less energy (at fixed velocity) to move the ellipsoid through the fluid with its long principal axis aligned with the flow, than with this axis perpendicular to the flow. This leads to coupling of the rotational motion to the translational motion. In the bulk, the rotational axis will precess about the velocity vector, and this would be expected to produce re-orientational dephasing of a molecular ro-vibrational absorption line, since there is a distribution of molecular translational velocity.

In order to derive the quantum hamiltonian for the motion of such an ellipsoid, we need to re-express the kinetic energy in terms of the momentum of the ellipsoid, defined by:

$$\mathbf{p} = \nabla_{\mathbf{v}} T = [M + M' \gamma_1] \mathbf{v} + M' (\alpha_1 - \gamma_1) (\boldsymbol{\lambda} \cdot \mathbf{v}) \boldsymbol{\lambda}, \quad (60)$$

which can be inverted to write

$$\mathbf{v} = \frac{1}{M + M' \gamma_1} \left[\mathbf{p} - \frac{M' (\alpha_1 - \gamma_1) (\boldsymbol{\lambda} \cdot \mathbf{p})}{M + M' \alpha_1} \boldsymbol{\lambda} \right]. \quad (61)$$

Substituting into the above expression for the kinetic energy gives

$$T = \frac{1}{2(M + M' \gamma_1)} \mathbf{p} \cdot \mathbf{p} - \frac{M' (\alpha_1 - \gamma_1)}{2(M + M' \alpha_1)(M + M' \gamma_1)} \times (\boldsymbol{\lambda} \cdot \mathbf{p})^2. \quad (62)$$

Making the substitution $\mathbf{p} \rightarrow i\hbar \nabla$ we get the quantum hamiltonian:

$$\mathcal{H} = -\frac{\hbar^2}{2M_{\text{eff}}} \nabla^2 + C_{\text{H}} [(\boldsymbol{\lambda} \cdot \nabla)^2 - \frac{1}{3} \nabla^2] + B_{\text{eff}} J^2 + V(\mathbf{r}, \boldsymbol{\lambda}), \quad (63)$$

where

$$M_{\text{eff}} = \frac{3(M + M' \alpha_1)(M + M' \gamma_1)}{3M + 2M' \alpha_1 + M' \gamma_1}, \quad (64)$$

$$C_{\text{H}} = \frac{\hbar^2 M' (\alpha_1 - \gamma_1)}{2(M + M' \alpha_1)(M + M' \gamma_1)}. \quad (65)$$

For our model of HCN in He, $C_{\text{H}}/h = -0.772 \text{ GHz } \text{\AA}^2$, and $M_{\text{eff}} = 35.2 \text{ u}$.

Before considering the case of an impurity in a cluster, it is instructive to examine the case of a linear molecule impurity in bulk He, where the momentum is a good quantum number. If we assume that we can treat the hydrodynamic coupling by first order perturbation theory, the shift in

energy for a level j, m_j (with the quantization axis along the velocity), and translational kinetic energy E_{trans} , is given by:

$$E_{\text{hydro}}(j, m_j) = A_{\text{H}} E_{\text{trans}} \frac{j(j+1) - 3m_j^2}{(2j-1)(2j+3)}, \quad (66)$$

$$A_{\text{H}} = (-1) \left(\frac{2M' (\alpha_1 - \gamma_1)}{3M + 2M' \alpha_1 + M' \gamma_1} \right). \quad (67)$$

For the case of HCN, $A_{\text{H}} = 0.036$. The $j = 0 \rightarrow 1$ transition will be shifted by $+0.4 A_{\text{H}} E_{\text{trans}}$ and $-0.2 A_{\text{H}} E_{\text{trans}}$ for polarization parallel and perpendicular to the velocity vector of the impurity. The width of a $j \rightarrow j+1$ transition will scale as $1/j$. Figure 9 shows the calculated spectral lineshapes for the R(0) and R(2) transitions after averaging over the Maxwell-Boltzmann distribution for E_{trans} . The horizontal axis is in units of $A_{\text{H}} k_{\text{b}} T_{\text{c}} / h^{-1}$ which equals 283 MHz for the case of HCN. The spectra have a cusp in the centre due to the $E_{\text{trans}}^{1/2}$ factor in the density of states. The higher frequency lobe arises from parallel transitions and the lower lobe, the perpendicular transitions (relative to the impurity momentum vector). Note that molecules with the projection of the rotational angular momentum perpendicular to the centre-of-mass momentum are higher in energy than those with rotational angular momentum either parallel or antiparallel to the linear momentum. This is because in the constant momentum case, orientations with the linear molecule axis parallel to the linear momentum are higher in energy, due to the lower effective mass for that orientation.

Explicit expressions for the matrix elements of the hydrodynamic term can be derived from the relationships from the matrix elements of $\boldsymbol{\lambda} \cdot \nabla$ operating on the spherical harmonics, as given by Rose [36]. After *considerable* algebra, the matrix elements diagonal in j in the coupled representation (where L is the centre-of-mass motion orbital angular momentum quantum number, j the quantum number of rotation of the linear impurity, and J the quantum number for the total angular momentum of the impurity),

$$\begin{aligned} \langle n, L, j, J, M \rangle &= \sum_{m_1, m_2} (-1)^{L-j+M} (2J+1)^{1/2} \\ &\times \begin{pmatrix} L & j & J \\ m_1 & m_2 & -M \end{pmatrix} \frac{\chi_{n,L}}{r} \\ &\times Y_{L, m_1}(\Omega) Y_{j, m_2}(\Omega_{\text{r}}) \end{aligned} \quad (68)$$

can be found. For $L' = L + 2$ they are:

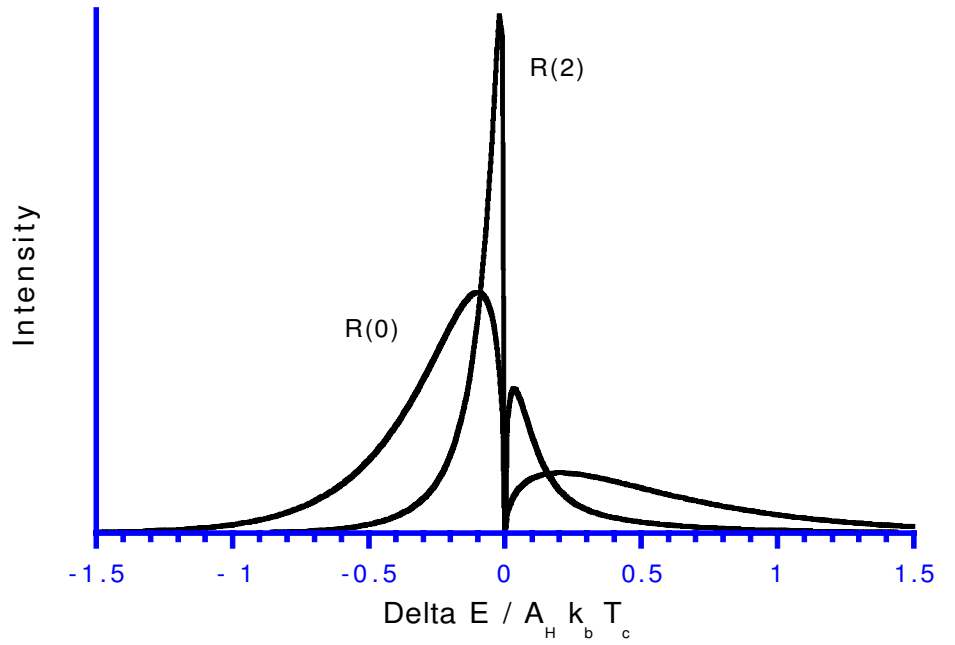


Figure 9. Calculated spectrum for the R(0) and R(2) lines of a linear molecule in bulk liquid He. The ordinate is plotted in units of $A_H k_b T_c h^{-1}$, where A_H is defined in the text, T_c the temperature of the liquid He, and the rest are standard symbols for physical constants.

$$\begin{aligned}
 & \langle n', L+2, j, J, M | (\boldsymbol{\lambda} \cdot \nabla)^2 - \frac{1}{3} \nabla^2 | n, L, j, J, M \rangle \\
 &= (-1) [(L+1)(L+2)]^{1/2} \\
 & \times \left[(j+1) \begin{Bmatrix} J & L & j \\ 1 & j+1 & L+1 \end{Bmatrix} \begin{Bmatrix} J & L+1 & j+1 \\ 1 & j & L+2 \end{Bmatrix} \right. \\
 & \left. + j \begin{Bmatrix} J & L & j \\ 1 & j-1 & L+1 \end{Bmatrix} \begin{Bmatrix} J & L+1 & j-1 \\ 1 & j & L+2 \end{Bmatrix} \right] \\
 & \times \int_0^R \chi_{n', L+2}(r) \left[\left(\frac{2M_{\text{eff}}}{\hbar^2} \right) (V(r) - E_{n,L}^0) \right. \\
 & \left. + \frac{(L+1)(2L+3)}{r^2} - \frac{2L+3}{r} \frac{d}{dr} \right] \chi_{n,L}(r) dr.
 \end{aligned}$$

For $L' = L-2$ they are:

$$\begin{aligned}
 & \langle n', L-2, j, J, M | (\boldsymbol{\lambda} \cdot \nabla)^2 - \frac{1}{3} \nabla^2 | n, L, j, J, M \rangle \\
 &= (-1) [L(L-1)]^{1/2} \\
 & \times \left[(j+1) \begin{Bmatrix} J & L & j \\ 1 & j+1 & L-1 \end{Bmatrix} \begin{Bmatrix} J & L-1 & j+1 \\ 1 & j & L-2 \end{Bmatrix} \right. \\
 & \left. + j \begin{Bmatrix} J & L & j \\ 1 & j-1 & L-1 \end{Bmatrix} \begin{Bmatrix} J & L-1 & j-1 \\ 1 & j & L-2 \end{Bmatrix} \right] \\
 & \times \int_0^R \chi_{n', L-2}(r) \left[\left(\frac{2M_{\text{eff}}}{\hbar^2} \right) (V(r) - E_{n,L}^0) \right. \\
 & \left. + \frac{L(2L-1)}{r^2} + \frac{2L-1}{r} \frac{d}{dr} \right] \chi_{n,L}(r) dr \quad (70)
 \end{aligned}$$

and for the case $L' = L$ they are:

$$\begin{aligned}
 & \langle n', L, j, J, M | (\boldsymbol{\lambda} \cdot \nabla)^2 - \frac{1}{3} \nabla^2 | n, L, j, J, M \rangle \\
 &= \left[(L+1)(j+1) \left| \begin{Bmatrix} J & L & j \\ 1 & j+1 & L+1 \end{Bmatrix} \right|^2 \right. \\
 & \left. + (L+1)j \left| \begin{Bmatrix} J & L & j \\ 1 & j-1 & L+1 \end{Bmatrix} \right|^2 \right. \\
 & \left. + L(j+1) \left| \begin{Bmatrix} J & L & j \\ 1 & j+1 & L-1 \end{Bmatrix} \right|^2 \right. \\
 & \left. + Lj \left| \begin{Bmatrix} J & L & j \\ 1 & j-1 & L-1 \end{Bmatrix} \right|^2 - \frac{1}{3} \right] \\
 & \times \int_0^R \chi_{n', L}(r) \left[\left(\frac{2M_{\text{eff}}}{\hbar^2} \right) (V(r) - E_{n,L}^0) \right] \chi_{n,L}(r) dr. \quad (71)
 \end{aligned}$$

For the case $j=0$, $J=L=L'$, and the matrix element reduces to:

$$\langle n', L, 0, L, M | (\boldsymbol{\lambda} \cdot \nabla)^2 - \frac{1}{3} \nabla^2 | n, L, 0, L, M \rangle = 0. \quad (72)$$

which is the reason that the $-\frac{1}{3} \nabla^2$ term was included as part of the hydrodynamic term. $V(r)$ is the isotropic part of $V(\mathbf{r}, \boldsymbol{\lambda})$ and the basis states are assumed to be eigenstates of \mathcal{H}_0 defined by:

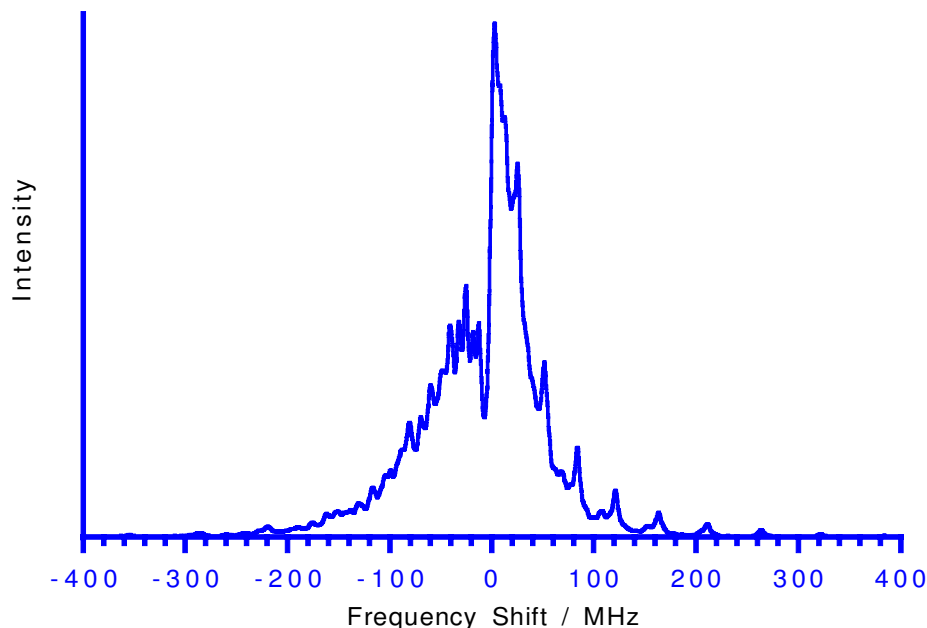


Figure 10. Calculated HCN R(0) line shape, including the isotropic term in the potential and the hydrodynamic coupling, for a He cluster of $R = 3$ nm.

$$\mathcal{H}_0 = -\frac{\hbar^2}{2M_{\text{eff}}}\nabla^2 + V(r) \quad (73)$$

with eigenvalues $E_{n,L}^0$. While not obvious by inspection, the above matrix elements can be shown to describe a Hermitian operator, as they should.

Using this hamiltonian, the $j = 0 \rightarrow 1$ spectrum of HCN in a He cluster can be recalculated. Figure 10 shows the spectrum calculated including the isotropic (C_{60}) term in the potential and the hydrodynamic coupling, but without the anisotropic potential term (C_{62}) for a cluster of $R = 3$ nm. The calculated spectrum of the impurity in the cluster looks remarkably like that (see figure 9) for a linear molecule impurity in bulk liquid He, except the spectrum is ‘inverted’. This can be understood as a consequence of averaging over the classical trajectory of the motion, which is in a plane perpendicular to L . For circular orbits, this leads to the prediction that the $j = 1$ state with $m_j = 0$ is higher in energy than the states with $m_j = \pm 1$ by an amount equal to $2(-C_{\text{H}})M_{\text{eff}}E_{\text{k}}/5\hbar^2$, where E_{k} is the average kinetic energy for the centre-of-mass motion. Using the thermal RMS kinetic energy, this gives a predicted average splitting of ≈ 150 MHz. This naturally explains the shape of the predicted spectrum and the energy scale.

Figure 11 shows the calculated cluster spectrum for the HCN R(0) line including both the anisotropic potential term and the hydrodynamic coupling. Somewhat surprisingly, the spectrum is narrower than for the case of either coupling term by itself. The reason is that for the dominant $\Delta L = 0$ matrix elements, the two sets of matrix elements destructively interfere. This is despite the fact that the two coupling terms are

complementary in that the hydrodynamic coupling is most important when the impurity is near the centre of the cluster (and thus has the highest velocity), while the potential anisotropy is most important at the outer turning point of the motion. The quantitative effect of this interference on the predicted spectrum will be a strong function of the particular parameters used in the calculation, including the cluster size.

7. Application to the R(0) transition of OCS

We will now consider the application of the present model to the case of OCS as an impurity, partly because of the elegant studies of the spectrum of this molecule performed in Göttingen, and also because it has the narrowest lines presently observed for an impurity in ^4He clusters [8]. In fact, the linewidths estimated above for the R(0) transition of HCN, while being well below that observed in the R(0) transition HCN in the first C–H overtone band, are similar to that of the R(0) line of the OCS ν_3 fundamental. This suggests that the present model may be more accurate in this case.

At the author’s request, Howson and Hutson have calculated long range coefficients for the He–OCS pair [37]. They find $C_{60} = 14.2\text{eV}\text{\AA}^6$, $C_{62} = 2.44\text{eV}\text{\AA}^6$, $C_{71} = 14.4\text{eV}\text{\AA}^7$ and $C_{73} = 13.9\text{eV}\text{\AA}^7$. Calculations were done with a number of basis sets, but the above results were done with a Dunning augmented-cc-pVTZ basis and are reported to have $\approx 10\%$ uncertainty. The calculations use self-consistent field (SCF) polarizabilities and employed the CADPAC6.3 program package.

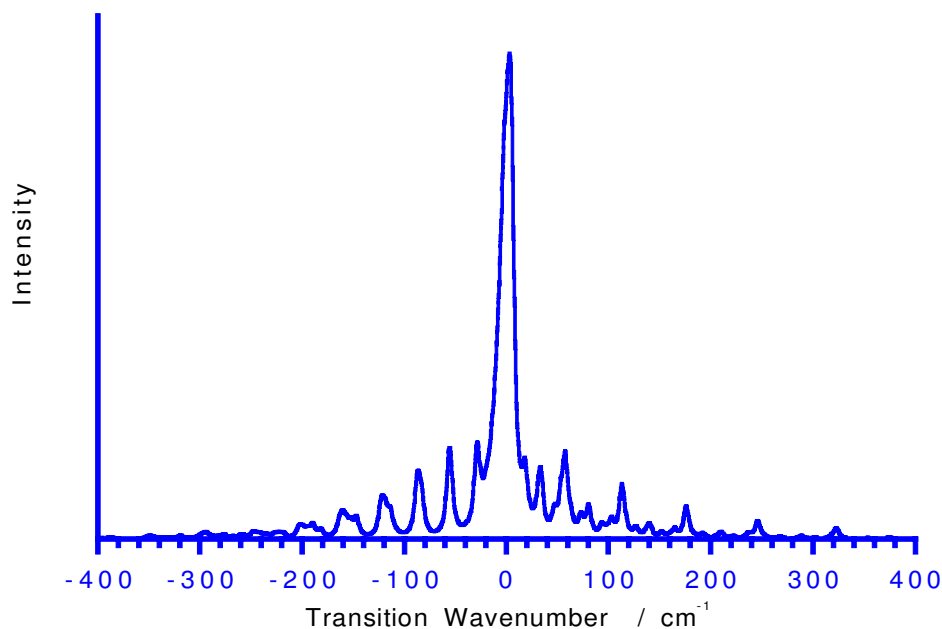


Figure 11 Calculated HCN R(0) line, including the isotropic and anisotropic terms in the potentials and the hydrodynamic coupling, for a He cluster of $R = 3$ nm.

In the present paper, we will continue to use only the lowest order, C_6 , terms, although the type of scaling done above indicates that the C_7 term may make a substantial contribution in the present case. Higgins and Klemperer [38] have calculated a series of points on the He–OCS surface at the MP4 level of theory, which they kindly made available to the author. From the position of the minimum as a function of angle between the He–OCS vector and the OCS molecular axis, we approximate the molecule as an ellipsoid with $a = b = 3.4 \text{ \AA}$ and $c = 4.7 \text{ \AA}$, or $\xi = 1.38$.

Figure 12 shows the R(0) transition of OCS observed in ^4He clusters, as reported by Grebenev *et al.* [14]. It has a FWHM of 150 MHz, and is asymmetric with a broad shoulder going to lower frequencies. Also in figure 12 is plotted the R(0) transition for OCS, predicted from the above parameters, and convoluted with a Lorentzian of 30 MHz FWHM to wash out most of the fine structure in the predicted spectrum. This is justified both because we expect vibrational and rotational relaxation lifetime to broaden the lines, and because the average over the cluster size distribution should at least partially wash out the high resolution structure. The agreement with experiment is remarkable, especially considering the uncertainty in the parameters going into the model. The calculated linewidth is somewhat too small, but the shape of the peak is in excellent agreement with what was observed in the experiment. This level of agreement is highly suggestive that the interactions included in the present model are the principal source of line broadening in the OCS R(0) transition. However, it must be noted that the experiments

have shown that the linewidth of the ro-vibrational lines increases dramatically with J , with the R(0) line being the narrowest. While the author has not calculated lineshapes for higher J transitions because of memory limitations on the personal computer on which these calculations have been performed, it is likely that the present model will not predict an increase in linewidth with J , but will more likely predict the opposite. Also the experiments show a significant difference in linewidth for the R(0) and P(1) lines, which should have the same lineshape (except for an inversion) in the present model, and in fact any model that does not include a vibrational dependence to the He–impurity interaction. We conclude that while the interactions considered in this paper likely play an important role in the lineshape of the R(0) transition, as yet unidentified interactions also play an important role, especially at higher J .

8. Hydrodynamic contribution to the effective moment of inertia

Let us now consider the hydrodynamic effect on the effective moment of inertia for rotation of our symmetric top impurity. It has been established experimentally that molecules rotate in liquid He clusters with an effective rotational constant that is smaller than that of the same molecule in the gas phase. This implies an increase in the effective moment of inertia for rotation. For light impurities with large rotational constants, fractional change of the rotational constants is small. For example, in the case of H_2O , the rotational constants in the cluster are almost identical with the gas phase [9]. In contrast, heavy impurities with small gas

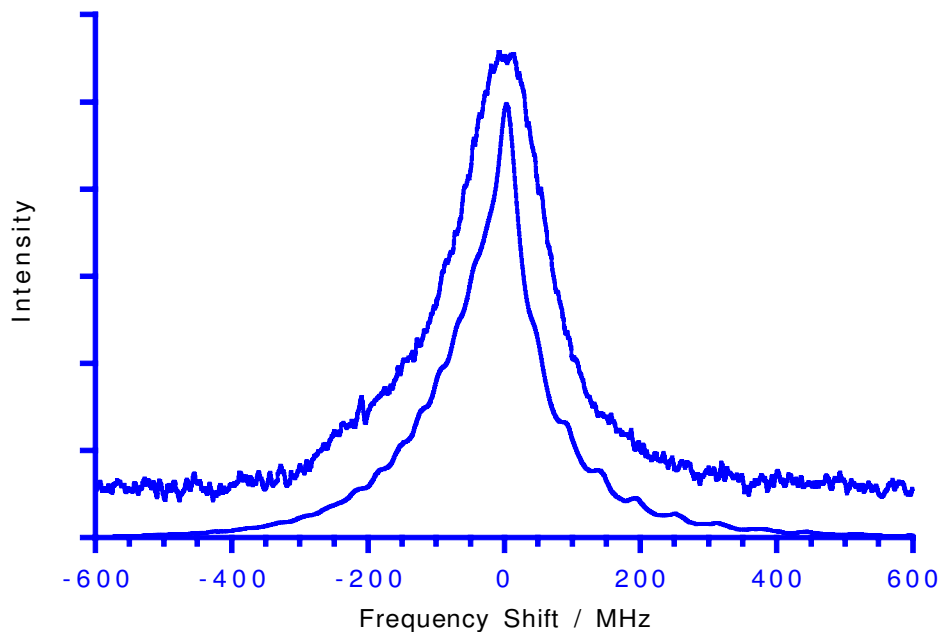


Figure 12. Plot of $R(0)$ line of the ν_3 fundamental band of OCS in a ${}^4\text{He}$ cluster of mean size $N = 2700$ ($R = 3.1$ nm). Taken from [14]. Also included is the calculated lineshape using anisotropic potential and hydrodynamic coupling, as described in the text, convoluted with a Lorentzian of 30 MHz FWHM.

phase rotational constants, such as $(\text{CH}_3)_3\text{SiCCH}$ have a rotational constant in the cluster of only $\approx 20\%$ as large as in the gas phase [4]. Some reduction in rotational constant is expected because of hydrodynamic effects, i.e. He must move out of the way of the rotating impurity, which contributes to the kinetic energy. Using the model of the impurity as an ellipsoid, we can directly calculate this increased moment of inertia from the size and shape of the molecule. The velocity potential for such motion is given by Milne-Thomson. Only an integral over the surface of the ellipsoid is needed to calculate the hydrodynamic contribution to the rotational kinetic energy. This leads to the following result for the hydrodynamic contribution to the moment of inertia for rotation about the axis perpendicular to the symmetry axis of the ellipsoid:

$$\Delta I_B = I' \Delta(\xi) + M' \gamma_1 r_{\text{com}}^2, \quad (74)$$

$$I' = \frac{1}{5} M' a^2 (1 + \xi^2), \quad (75)$$

$$\Delta(\xi) = \frac{1}{1 + \xi^2} \frac{(1 - \xi^2)^2 (\alpha_0 - \gamma_0)}{2(1 - \xi^2) - (1 + \xi^2)(\alpha_0 - \gamma_0)}. \quad (76)$$

r_{com} is the displacement of the impurity centre of mass from the geometric centre of the ellipsoid and I' is the value of I_B for the ellipsoid if filled with liquid He and this provides the natural scale for the effect. The other symbols are as defined above. Figure 13 shows a plot of $\Delta(\xi)$ as a function of ξ . For $\xi \approx 1$, one can use the expansion $\Delta(\xi) \approx \frac{2}{3}(\xi - 1)^2$.

As an application of this expression, we will again consider OCS. Using the parameters that $a = b = 3.4 \text{ \AA}$ and $c = 4.7 \text{ \AA}$ estimated from the *ab initio*

points [38] and $r_{\text{com}} = 0.1 \text{ \AA}$, the calculated enhancement of the B moment of inertia is 9.33 u \AA^2 , compared to a value of $I_B = 83.1 \text{ u \AA}^2$, or a predicted rotational constant of OCS in the cluster of 90% of the gas phase value. This is a small fraction of the observed reduction in B , where the observed B value in He clusters is 36% of the gas phase B value [8].

Note added in proof: Recently, the author and his collaborators have demonstrated that quantitative agreement between experimentally measured and calculated reduction of B for OCS and several other molecules is obtained with a superfluid hydrodynamic model if the spatial variation of the helium density around the impurity molecule is taken into account [40].

Another model for the reduction of rotational constants is to assume a solvation shell of He atoms that rotate with the impurity. In the case of SF_6 , such a model seems to naturally explain the observed reduction in B [3], but does not naturally explain the observed value of the A rotational constant for $(\text{SF}_6)_2$ [8], which by such a model would be expected to be at least $\frac{1}{2}$ of the B value for the SF_6 monomer in the cluster, while the observed value (based upon a spectral fit) is less than $\frac{1}{4}$. In their recent paper on OCS in mixed ${}^3\text{He}$ and ${}^4\text{He}$ clusters, Grebenev *et al.* [6] propose a model for the effective rotational constants of impurities in He with a position dependent normal fluid density around the impurity that rotates with it and thus contributes to the moment of inertia. However, they give no microscopic description of how this normal fraction could be defined, nor how it could be measured, thus this model appears to lack empirical content at least until

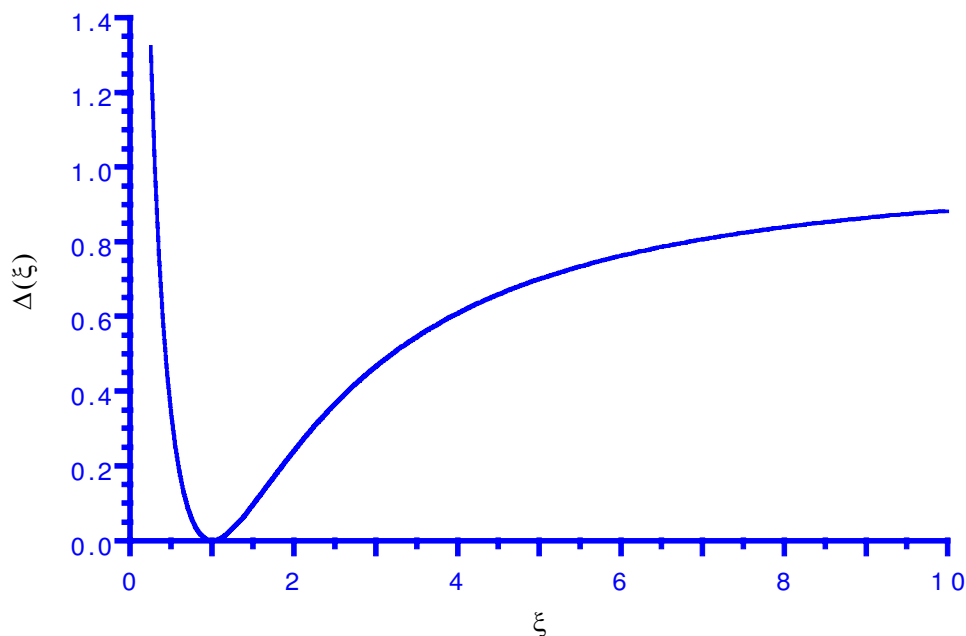


Figure 13. The hydrodynamic constant $\Delta(\xi)$ as a function of ξ . See equation (76) for the definition of this quantity.

it is more precisely defined. It is interesting to point out in this context that previous fully quantum microscopic calculations have found that He atoms in the first solvation shell about SF_6 participate in exchange and are thus part of the superfluid [39]. These authors did find that at 0.625 K the superfluid fraction in a $\text{SF}_6\text{He}_{39}$, 0.67(7), was less than previously calculated for a He_{64} cluster, 0.9(1). It would be interesting for these calculations to be repeated for larger He clusters (at least enough to ‘fill’ the second solvation shell around the SF_6), and at a temperature near that found for experimental clusters in order to make better contact with the presently available spectroscopic experiments.

9. Summary

In this paper, we have considered the energetics and dynamics for the motion of impurities in spherical liquid ^4He clusters, which are treated as superfluid liquid droplets. It is found that the effective potential for motion of the impurity is determined by the long range part of the impurity–He interaction. The isotropic part ‘traps’ the impurity near the centre of the cluster. The anisotropic part results in a coupling of the rotation and centre-of-mass motion of the impurity, which leads to inhomogeneous broadening in the predicted IR and microwave spectra. Calculated broadening values are on the order of 0.1 GHz, on the order of the narrowest lines observed in IR spectroscopy of impurities in liquid He. Hydrodynamic effects are also found to play an important role by coupling molecular rotation to the velocity of centre-of-mass motion. The inhomogeneous spectral effects of the distribution of thermally excited ripplons are found

to be much smaller and are likely negligible in determining linewidths, though they likely play an important role in determining the time required for the impurity and cluster to come into equilibrium. Direct hydrodynamic effects are found to make a minor contribution to the dramatic reductions in effective rotational constants often found for impurity species in He cluster spectroscopy.

This work will surely not be the last word on this subject. The interactions considered here, while certainly present, do not appear to be sufficiently strong to explain the observed linewidths of many impurities, such as SF_6 and HCN. This suggests other, perhaps more subtle, physical effects are playing a role. New nonlinear spectroscopic experiments that use either pump-probe methods and/or spectral hole burning are clearly needed to sort out homogeneous and inhomogeneous effects in He cluster spectroscopy and to provide critical tests of simple models. Microscopic theory will also surely play an important role in helping to sort out the various physical effects that can play a role.

The He cluster research at Princeton was carried out with support from the Air Force High Density Materials program and the National Science Foundation. The author would like to acknowledge Professor Giacinto Scoles for many helpful discussions about intermolecular potentials and for inviting the author to join his research effort on He clusters. Kelly Higgins and William Klemperer as well as J. P. Toennies and his co-workers are acknowledged for making their results available prior to publication. Joanna Howson and

Jerry Hutson are noted for kindly calculating the long range interaction constants for He–OCS. Carlo Callegari, Irene Reinhard and Andrej Vilesov are noted for their careful reading of this manuscript, which helped greatly to improve the final version. The hospitality and support of JILA, where the work was completed and the paper written, is also acknowledged.

References

- [1] WHALEY, K. B., 1998, *Advances in Molecular Vibrations and Collision Dynamics*, Vol. III, edited by J. Bowman (Greenwich, Conn.: JAI Press, Inc.).
- [2] LEHMANN, K. K., and SCOLES, G., 1998, *Science*, **279**, 2065.
- [3] HARTMANN, M., MILLER, R. E., TOENNIES, J. P., and VILESOV, A. F., 1996, *Science*, **272**, 1631.
- [4] CALLEGARI, C., CONJUSTEAU, A., REINHARDT, I., LEHMANN, K. K., and SCOLES, G., 1998, unpublished work.
- [5] HIGGINS, J., ERNST, W., CALLEGARI, C., REHO, J., LEHMANN, K. K., SCOLES, G., and GUTOWSKI, M., 1996, *Phys. Rev. Lett.*, **77**, 4532.
- [6] GREBENEV, S., TOENNIES, J. P., and VILESOV, A. F., 1998, *Science*, **279**, 2083.
- [7] ANDRONIKASHVILI, E. L., 1946, *J. Phys. USSR*, **10**, 201.
- [8] HARTMANN, M., 1997, PhD thesis, University of Göttingen, Germany.
- [9] FRÖCHTENICHT, R., KALOUDIS, M., KOCH, M., and HUISKEN, F., 1996, *J. chem. Phys.*, **105**, 6128.
- [10] REINHARD, I., CALLEGARI, C., CONJUSTEAU, A., LEHMANN, K. K., and SCOLES, G., 1999, *Phys. Rev. Lett.*, **82**, 5036.
- [11] TOENNIES, J. P., and VILESOV, A. F., 1995, *Chem. Phys. Lett.*, **235**, 596.
- [12] BRINK, D. M., and STRINGARI, S., 1990, *Z. Phys. D*, **15**, 257.
- [13] LURIO, L. B., RABEDEAU, T. A., PERSHAN, P. S., SILVERA, I. F., DEUTSCH, M., KOSOWSKY, S. D., and OCKO, B. M., 1993, *Phys. Rev. B*, **48**, 4518.
- [14] GREBENEV, S., HARTMANN, M., HAVENITH, M., SARTAKOV, B., TOENNIES, J. P., and VILESOV, A. F., preprint (unpublished).
- [15] LEHMANN, K. K., and NORTHBY, J. A., 1999, *Molec. Phys.*, **97**, 639.
- [16] STANDARD, J. M., and CERTAIN, P. R., 1985, *J. chem. Phys.*, **83**, 3002.
- [17] PACK, R. T., 1982, *J. phys. Chem.*, **86**, 2794.
- [18] TELLINGHUISEN, J., 1988, *Int. J. quantum Chem.*, **34**, 401.
- [19] ATKINS, K. M., and HUTSON, J. M., 1996, *J. chem. Phys.*, **105**, 440.
- [20] DALGARNO, A., 1967, *Advances in Chemical Physics*, Vol. 12, edited by I. Prigogine and S. A. Rice (New York: Wiley), p. 143.
- [21] EICHENAUER, D., and LEROY, R. J., 1988, *J. chem. Phys.*, **88**, 2898.
- [22] TOWNES, C. H., and SCHAWLOW, A. L., 1955, *Microwave Spectroscopy* (New York: McGraw-Hill).
- [23] KUHN, H., and LONDON, F., 1934, *Phil. Mag.*, **18**, 983.
- [24] REDINGTON, R. L., and MILLIGAN, D. E., 1962, *J. chem. Phys.*, **37**, 2162.
- [25] REDINGTON, R. L., and MILLIGAN, D. E., 1963, *J. chem. Phys.*, **39**, 3430.
- [26] FRIEDMANN, H., and KIMEL, S., 1965, *J. chem. Phys.*, **43**, 3925.
- [27] FRIEDMANN, H., and KIMEL, S., 1967, *J. chem. Phys.*, **47**, 3589.
- [28] EDMONDS, A. R., 1960, *Angular Momentum in Quantum Mechanics*, 2nd Edn (Princeton, NJ: Princeton University Press).
- [29] ZARE, R. N., 1988, *Angular Momentum: Understanding Spatial Aspects in Chemistry and Physics* (Ithaca, NY: Wiley).
- [30] NAUTA, K., and MILLER, R. E., 1999, *Phys. Rev. Lett.*, **82**, 4480.
- [31] SIENKEMEIER, F., HIGGINS, J., ERNST, W. E., and SCOLES, G., 1995, *Z. Phys. B*, **98**, 413.
- [32] HARTMANN, M., MIELKE, F., TOENNIES, J. P., VILESOV, A. F., and BENEDEK, G., 1996, *Phys. Rev. Lett.*, **76**, 4560.
- [33] LAMB, H., 1916, *Hydrodynamics*, 4th Edn (Cambridge: Cambridge University Press).
- [34] ELSER, V., and PLATZMAN, P. M., 1988, *Phys. Rev. Lett.*, **61**, 177.
- [35] MILNE-THOMSON, L. M., 1996, *Theoretical Hydrodynamics*, 5th Edn (New York: Dover).
- [36] ROSE, M. E., 1954, *Proc. phys. Soc.*, **67A**, 239.
- [37] HOWSON, J. M. M., and HUTSON, J. M., 1998, private correspondence.
- [38] HIGGINS, K., and KLEMPERER, W., 1999, *J. chem. Phys.*, **110**, 1383.
- [39] KWON, Y., CEPERLEY, D. M., and WHALEY, K. B., 1996, *J. chem. Phys.*, **104**, 2341.
- [40] CALLEGARI, C., CONJUSTEAU, A., REINHARD, I., LEHMANN, K. K., SCOLES, G., and DALFOVO, F., 1999, manuscript in preparation.